Light-activated cartilage decellularised extracellular matrix hydrogels for engineering chondrogenic microenvironments with localised oxygen control

Biofabrication

OPEN ACCESS

RECEIVED
9 January 2026

REVISED
6 April 2026

ACCEPTED FOR PUBLICATION
20 April 2026

PUBLISHED
8 May 2026

PAPER

Light-activated cartilage decellularised extracellular matrix hydrogels for engineering chondrogenic microenvironments with localised oxygen control

Lin Li[1,2], **Louis Jun Ye Ong**[1,2,3,4], **Khoon S Lim**[5,6], **Chamikara Liyanage**[7], **Yunkun Qu**[1,2], **Jingyi Wen**[1,2], **Caitlin Williams**[8,9], **Thomas G Molley**[9,10], **Roberto A Barrero**[11], **Shital Wakale**[1,2], **Ross Crawford**[1,12], **Kristopher A Kilian**[8,9,10], **Yi-Chin Toh**[1,2,3,*] and **Indira Prasadam**[1,2,*]

[1] Centre for Biomedical Technologies, Queensland University of Technology, Brisbane 4059, Australia
[2] School of Mechanical, Medical & Process Engineering, Queensland University of Technology, Brisbane 4059, Australia
[3] Max Planck Queensland Centre (MPQC) for the Materials Science of Extracellular Matrices, Queensland University of Technology, Brisbane 4000, Australia
[4] School of Applied Sciences, Temasek Polytechnic, Singapore 529757, Singapore
[5] School of Medical Sciences, University of Sydney, Sydney, NSW 2006, Australia
[6] Sydney Biomanufacturing Incubator, University of Sydney, Sydney, NSW 2006, Australia
[7] School of Biomedical Sciences, Faculty of Health, Queensland University of Technology, Brisbane, QLD 4059, Australia
[8] School of Chemistry, Australian Centre for NanoMedicine, UNSW Sydney, Sydney 2052, Australia
[9] School of Materials Science and Engineering, UNSW Sydney, Sydney 2052, Australia
[10] OxyLo Inc., San Diego, CA, United States of America
[11] eResearch, Research Infrastructure, Academic Division, Queensland University of Technology, Brisbane, QLD 4001, Australia
[12] Department of Orthopaedics, The Prince Charles Hospital, Brisbane 4032, Australia
[*] Authors to whom any correspondence should be addressed.

E-mail: yichin.toh@qut.edu.au and i.prasadam@qut.edu.au

Keywords: decellularised cartilage extracellular matrix, photo-crosslinked hydrogel, hBMSC, chondrogenic differentiation, hypoxia

Supplementary material for this article is available online

Abstract

Cartilage tissue engineering requires biomaterials that can effectively maintain the tissue-specific functions of chondrocytes to enable the restoration of cartilage structure and function. Decellularised extracellular matrix (dECM)-derived hydrogels serve as tissue-specific biomaterials capable of preserving native biochemical cues and maintaining physiological chondrocyte phenotype in three-dimensional culture. However, their sol-gel transition relies heavily on collagen fibrillogenesis, a slow and poorly controllable process that limits mechanical tunability and suffers from inter-batch variability. Therefore, further efforts are required to functionalise cartilage dECM to achieve reproducible and controllable physicochemical properties. Here, we present a light-activated cartilage dECM hydrogel system based on ruthenium/sodium persulfate (Ru/SPS)-mediated dityrosine crosslinking, enabling rapid hydrogel formation under visible light irradiation while providing tunable mechanical properties and improved biological functionality. Comparison of the decellularisation protocols indicated that Triton X-100 combined with ammonium hydroxide efficiently eliminated residual DNA while preserving a substantial proportion of the native cartilage proteome. Pepsin-solubilised cartilage dECM hydrogels formed via dityrosine-based photo-crosslinking exhibited rapid gelation behaviour and superior mechanical characteristics compared to conventional thermally gelled dECM. The photo-crosslinked dECM hydrogels were cytocompatible, supported human bone marrow-derived mesenchymal stem cells (hBMSCs), and favoured cartilage-specific phenotypes, as demonstrated by the upregulation of chondrogenic genes, including *COL2A1* and *ACAN*, compared with gelatin methacrylate (GelMA) hydrogels. Importantly, this photo-crosslinking strategy overcomes the incompatibility between oxygen-sensitive redox-based photochemistry and hypoxic culture conditions, enabling the incorporation of oxygen-scavenging microcapsules to establish low-oxygen microenvironments. Under hypoxia, the cartilage dECM hydrogels promoted a more articular-like phenotype in hBMSC-derived chondrocytes,

with transcriptomic features associated with TGF-β/SMAD2/3 and IGF-1/2–IGF-1R signalling. Collectively, these findings establish photo-crosslinked cartilage dECM hydrogels as a biomaterial platform with tunable mechanical properties and favourable biological functionality for cartilage tissue bioengineering and biomimetic *in vitro* cartilage models.

1. Introduction

Decellularised extracellular matrix (dECM) is a class of biomaterials derived from multiple tissue types and hence preserves native biochemical cues capable of maintaining tissue-specific cell function in three-dimensional (3D) *in vitro* cultures [1, 2]. For cartilage tissue engineering applications, dECM-derived hydrogels have demonstrated improved capacity to sustain chondrogenic phenotype relative to widely used matrices such as gelatin methacrylate (GelMA) [3]. Conventionally, cartilage dECM hydrogels are produced by tissue decellularisation followed by enzymatic solubilisation and collagen fibrillogenesis [4]. However, due to the difficulty in controlling fibrillogenesis-based crosslinking and the sensitivity of fibril architecture and mechanical properties to processing conditions, dECM hydrogels often exhibit variability in hydrogel formation and material properties, together with limited mechanical stiffness, which may compromise their ability to support chondrogenic differentiation [5–7]. Therefore, new strategies are required to better control dECM hydrogel properties while preserving biological activity.

Functionalisation of cartilage-derived dECM is required to achieve reproducible and tunable physicochemical properties while preserving native biological fidelity. To address these limitations, physical reinforcement strategies (e.g. support baths, sacrificial hydrogels, nanofibres) and chemical modifications (e.g. genipin crosslinking, methacrylation, polymer blending) have been explored to address these limitations, but they often introduce additional processing complexity or require prior matrix modification, which may compromise native dECM features [6, 8–11]. Photo-crosslinking is widely adopted due to its rapid, spatiotemporally controllable gelation, compatibility with cell-laden biofabrication, and ability to decouple processing from bulk chemistry under mild, aqueous conditions. The ruthenium (Ru)/sodium persulfate (SPS) visible-light photoinitiator system has gained considerable attention due to its ability to avoid ultraviolet (UV)-associated DNA damage, achieve efficient polymerisation at low initiator concentrations, permit deeper light penetration for uniform crosslinking of bulky constructs, and improve glycosaminoglycan (GAG) deposition and redifferentiation in chondrocyte-laden constructs relative to lithium phenyl (2,4,6-trimethylbenzoyl) phosphinate (LAP)-based crosslinking [12–14].

In cartilage tissue engineering, oxygen control is particularly important because physiological hypoxia (2%–5% O_2) plays a key role in maintaining chondrocyte phenotype and promoting chondrogenic differentiation [15, 16]. This consideration becomes especially relevant when oxygen-regulating components are incorporated into photo-crosslinkable hydrogel systems, as localised oxygen depletion may influence crosslinking performance and network stability [17–19]. Thus, despite advances in dECM hydrogel design, there remains a need for alternative photo-crosslinking strategies that enable rapid, robust, and tunable gelation under hypoxic conditions while preserving native ECM bioactivity. Addressing this gap requires hydrogel platforms that integrate mechanical tunability with regulation of the local oxygen microenvironment.

Here, we present a strategy that reconciles photo-crosslinking requirements with physiologically relevant oxygen tensions using a tyrosine-dependent Ru/SPS system, a visible-light-activated crosslinking chemistry that exploits endogenous tyrosine residues to form covalent protein–protein networks without chemical modification of dECM [12, 13, 20]. This system enables rapid gelation and tunable mechanical stiffness via photoinitiator concentration, making it well-suited for cartilage dECM. We further demonstrate compatibility with a microencapsulated glucose oxidase/catalase oxygen-scavenging system to establish controllable, localised hypoxic niches within the Ru/SPS cartilage dECM hydrogels [21]. To minimise biochemical variability affecting photo-crosslinking efficiency, bovine cartilage decellularisation was optimised through integrated biochemical, mechanical, and proteomic analyses to ensure consistent preservation of ECM components required for dityrosine bond formation. The resulting solubilised dECM was formulated into biomimetic 3D constructs using Ru/SPS photo-crosslinking, yielding bioactive hydrogels with tunable mechanics, improved handling, and scalability for high-throughput applications. Importantly, the combination of photo-crosslinked dECM and localised physiological hypoxia significantly enhances chondrogenic differentiation of human bone marrow-derived mesenchymal stem cells (hBMSCs) in 3D culture.

2. Materials and methods

2.1. Materials

Phosphate-buffered saline (PBS), penicillin-streptomycin (PS), amphotericin B, and low- and high-glucose Dulbecco's modified Eagle medium

(DMEM) were purchased from Gibco (USA). TRIzol reagent and 4′,6-diamidino-2-phenylindole (DAPI) were purchased from Invitrogen (USA). Sodium dodecyl sulphate (SDS), ammonium hydroxide (NH_4OH), paraformaldehyde (PFA), hexamethyldisilane (HMDS), Safranin O solution, chondroitin sulphate, bovine serum albumin (BSA), and pepsin were purchased from Sigma-Aldrich (Australia). Triton X-100, Tris, Entellan New Mounting Medium, tris(2,2′-bipyridyl) dichlororuthenium (II) hexahydrate (Ru), and sodium persulfate (SPS) were purchased from Merck (Australia). Tissue-Tek O.C.T. Compound was purchased from Sakura Finetek (USA). Hematoxylin and eosin (H&E) were purchased from HD Scientific (Australia), and Picrosirius red was purchased from Abcam (Australia). Red blood cell (RBC) lysis buffer was purchased from Fisher Scientific (Germany). Dithiothreitol (DTT), iodoacetamide (IAA), methanol, trypsin, ammonium bicarbonate (ABC) digestion buffer (pH 8.0), Lys-C, acetonitrile, formic acid, hydrochloric acid (HCl), sodium hydroxide (NaOH), Calcein AM, propidium iodide (PI), PrestoBlue reagent, the high-capacity complementary DNA (cDNA) reverse transcription kit, and SYBR Green PCR Master Mix were purchased from Thermo Fisher Scientific (Australia). Gelatin methacrylate (GelMA) was purchased from Engineering For Life (China). The DNeasy Blood & Tissue Kit was purchased from QIAGEN (Germany), and the Blyscan™ GAG assay kit was purchased from Bicolor (UK).

Primary hBMSCs were isolated from donor bone marrow collected from patients undergoing knee arthroplasty (aged 73, 65, and 54 years) under approval from the Queensland University of Technology and St Vincent's Private Hospital Human Research Ethics Committees (approval number: #1400001024). All procedures involving human participants were conducted in accordance with the Declaration of Helsinki, and written informed consent was obtained from all participants.

2.2. Decellularisation

The fresh bovine knee joint was obtained from a local butcher (Brisbane, Australia). Articular cartilage was dissected with scalpels, rinsed twice with PBS, and stored at −80 °C until further use [22]. Three decellularisation protocols were employed, utilising different concentrations of SDS and a combination of Triton X-100 and NH_4OH (table 1). Among the various decellularisation methods available, detergent-based protocols were selected owing to their relative procedural simplicity and widespread adoption in the literature [23, 24]. SDS is an ionic detergent recognised for its ability to disrupt cell membranes and solubilise cellular debris [23]. Protocols 1 and 2 differ in their respective SDS concentrations. Triton X-100 functions as a non-ionic detergent that assists decellularisation through the disruption of cellular membranes [25]. In protocol 3, NH_4OH was incorporated alongside Triton X-100, a combination commonly reported as an additive in decellularisation procedures [10].

Table 1. Overview of the decellularisation protocols evaluated in this study.

Protocol	Protocol description
1% SDS	1% SDS (w/v) for 1 d
2% SDS	2% SDS (w/v) for 1 d
1% Triton–0.1% NH_4OH	1% Triton X-100 (v/v) and 0.1% NH_4OH (v/v) for 2 d

Firstly, the cartilage tissue was embedded in Tissue-Tek O.C.T. Compound, frozen into a block, and then mounted onto the cryostat (Cryostar NX70, Thermo Fisher, Waltham, USA) for sectioning. The 10 μm-thick cartilage slices were then rinsed with distilled deionised water (DDW), weighed, and separated into three different protocols. Tissue samples were incubated with the respective decellularisation solutions in 50 ml Falcon tubes using appropriate volumes. The tubes were then placed on an orbital shaker at 4 °C, spinning at 100 rpm, and the detergent solution was replaced every 12 h. After decellularisation, samples were rinsed three times with DDW and then sterilised at 4 °C in a solution of 1% PS and 2.5 μg ml^{-1} amphotericin B in DDW. After sterilisation, samples underwent three additional rinses with DDW before being frozen at −80 °C overnight and subsequently lyophilised using a freeze dryer (CoolSafe 110–4, ScanVac, Allerød, Denmark) for 24 h. Throughout the experiment, tissue samples (∼10 mg) were preserved at −80 °C for later biochemical analyses, including DNA and proteomic quantification, as well as evaluation of structural composition. Alternatively, samples were fixed in 4% (w/v) PFA for histological examination or mechanical characterisation.

2.3. H&E staining

H&E staining was employed for the visualisation of residual nuclei. Samples were fixed in 4% PFA for 20 min, rinsed three times in PBS, and stored at 4 °C until further processing. Cartilage slices from different decellularisation conditions were selected and then subjected to H&E staining. After staining, the slides were mounted with Entellan New Mounting Medium and subsequently imaged at 40× magnification using a Pannoramic Scan digital slide scanner (3DHISTECH, Budapest, Hungary).

2.4. Safranin O staining

Safranin O staining was conducted to evaluate the preservation of GAGs following decellularisation. Tissue samples were fixed and stored according to the protocol outlined in section 2.3. Slides were processed with Safranin O solution and subsequently mounted and imaged as described above. Quantification of the

Safranin O-positive area was performed using ImageJ software.

2.5. DNA quantification

Double-stranded DNA (dsDNA) remaining in decellularised cartilage samples was extracted with the DNeasy Blood & Tissue Kit according to the manufacturer's protocol and subsequently quantified using a NanoDrop One^{C} spectrophotometer (Thermo Fisher Scientific, Waltham, USA).

2.6. GAG quantification

GAG content in papain-digested cartilage samples was measured using a Blyscan™ GAG assay kit following the manufacturer's instructions [26]. Absorbance of the digested samples was measured at 656 nm using a microplate reader (CLARIOstar, BMG Labtech, Ortenberg, Germany). GAG concentrations were analysed based on a standard curve generated using chondroitin sulphate prepared in sodium phosphate buffer over a range of 0–100 μg ml^{-1}.

2.7. DAPI staining

DAPI staining was performed to visualise residual nuclear material. Cartilage tissues were fixed and stored as described in section 2.3. Cartilage slides were stained with DAPI following the manufacturer's protocol. Fluorescence imaging was conducted using a 20× objective on a Leica TCS SP5 microscope (Leica Microsystems, Wetzlar, Germany).

2.8. Picrosirius red staining

To observe the collagen structure, we used picrosirius red staining combined with polarised light microscopy (PLM). Tissues were fixed and stored as previously described. Slides were imaged under PLM using a 10× objective (Olympus PLM slide scanner, Olympus, Tokyo, Japan).

2.9. Fourier transform infrared spectroscopy (FTIR) and spectral analysis

FTIR analysis was performed to characterise the biochemical composition of the samples. Tissues were first ground into a fine powder, and spectra were recorded using a Nicolet FTIR spectrometer (Thermo Electron Corp., Waltham, USA) equipped with a diamond attenuated total reflectance accessory. For each measurement, spectra were collected by averaging 64 scans over a wavenumber range of 4000–525 cm^{-1} with a resolution of 4 cm^{-1}.

2.10. Nanoindentation

The mechanical stiffness of cartilage tissues in an aqueous environment was assessed using nanoindentation [27]. Samples were prepared as described previously. Measurements were performed using a TI 950 TriboIndenter (Hysitron, Billerica, USA) equipped with a spherical indenter, with the samples submerged in PBS. Before testing, the instrument was calibrated using standard fused quartz and aluminium specimens. Experimental conditions included a preload of 1 μN, a peak load of 30 μN, and a loading time of 3 s. The elastic modulus, representing cartilage stiffness, was calculated from the unloading segment of the load–displacement curve using the Oliver–Pharr method [28]. In this context, a higher modulus reflects increased stiffness of the cartilage matrix. The reduced modulus (E_r) was determined using the standard equations and represents the effective elastic modulus of the cartilage tissue while accounting for elastic deformation of both the specimen and the indenter, as indicated in equation (1) [27],

$$\frac{1}{E_r} = \frac{\left(1-\nu^2\right)}{E} + \frac{\left(1-\nu_i^2\right)}{E_i} \tag{1}$$

E and ν are the Young's modulus and Poisson's ratio of the tested sample, respectively. E_i and ν_i represent the elastic modulus and Poisson's ratio of the indenter tip, respectively ($E_i = 1440$ GPa, $\nu_i = 0.07$) [29].

2.11. Scanning electron microscopy (SEM)

Samples were initially fixed in 4% PFA for 20 min, washed three times with PBS, and stored at 4 °C. The sections were subsequently dehydrated using a stepwise ethanol gradient (20%–100%). This was followed by further dehydration using HMDS. Subsequently, the samples were sputter-coated with gold to enhance conductivity. Finally, the prepared samples were imaged using a Tescan Mira 3 SEM (Tescan, Brno, Czech Republic).

2.12. Proteomics analysis

The lyophilised cartilage samples were weighed and ground into a fine powder for proteomic analysis. Our procedure for proteolytic digestion follows the established method provided by the S-Trap™ micro spin column digestion protocol [30]. In brief, for protein handling, the S-Trap™ Micro was used, which accommodates 50–100 μg of protein. Cartilage tissues were first lysed using SDS lysis buffer (10% SDS, 100 mM Tris), with 25 μl of buffer added to 25 μg of sample. Subsequently, 25 μl of the lysate was transferred to a fresh tube containing 4 μl DTT (500 mM in water), resulting in a final DTT concentration of 20 mM. The mixture was incubated at 70 °C for 60 min and then allowed to cool to room temperature. Cysteine was alkylated by adding 8 μl IAA for a final concentration of 40 mM, followed by a 30 min incubation in the dark. If DNA was present, it was sheared through sonication. To the lysate in 25 μl SDS buffer, 2.5 μl 12% phosphoric acid was added, followed by mixing with 165 μl of S-Trap binding buffer (90% aqueous methanol, 100 mM Tris). The sample was clarified by centrifugation for 8 min at

13 000 g if needed. The entire sample was transferred to the spin column, ensuring it did not overflow, and centrifuged at 4000 g for 1 min, repeating as necessary. The column was washed three times with 150 μl S-Trap binding buffer, with the flow-through discarded each time. The S-Trap was transferred to a new collection tube. Trypsin was added at 1 μg or a 1:50–1:100 ratio (w/w) in 50 μl of 50 mM digestion buffer (ABC, pH 8.0) to the protein trap, avoiding air bubbles. Optionally, 0.5 μg Lys-C was added, followed by trypsin in staggered doses. The loosely capped spin column was incubated in a closed bag with moist tissue either at 47 °C for 1 h or overnight at 37 °C without shaking. Peptides were eluted sequentially with 40 μl of 5%, 50%, and 75% acetonitrile in 0.1% formic acid, collecting all eluents in the same tube. The top 100 μl was transferred into a plastic insert, dried in a speed-vac centrifuge, then resuspended in 20 μl buffer A. The peptides obtained were analysed by nano ultra-high-performance liquid chromatography (nano UHPLC, Ultimate 3000 RSLC, Thermo Fisher Scientific, Waltham, USA). This system was effectively integrated with an Orbitrap Exploris 480 mass spectrometer (Thermo Fisher Scientific, Waltham, USA). Peptides were separated using a nanoEase M/Z Peptide CSH C18 column (130 Å, 1.7 μm, 300 μm × 100 mm; Waters, Milford, USA), which provides high precision and efficient peptide separation for subsequent characterisation.

2.13. LC-MS/MS data analysis

Protein abundance values from all replicates were processed using the MetaboAnalyst 5.0 online platform, following previously reported procedures [31, 32]. Log_2-transformed and normalised datasets were used for principal component analysis, focusing on the first three principal components. Heatmaps were constructed based on normalised protein intensities and clustered using Ward's linkage method, while hierarchical clustering with Euclidean distance determined the ordering of rows and columns. Fold changes in protein abundance between experimental groups were calculated using $\log_2$ transformation. Differentially expressed proteins (DEPs) were defined using thresholds of $|\log_2$ fold change (FC)$| \geqslant 0.5$ and $p \leqslant 0.05$. These proteins were subsequently analysed using Ingenuity Pathway Analysis (IPA) to identify significantly altered canonical signalling pathways and upstream regulators [32, 33]. Dysregulated pathways were determined using a Z-score cutoff of ± 1.50 with $p \leqslant 0.05$.

2.14. dECM solubilisation

For dECM digestion, lyophilised cartilage tissues were subjected to 0.1 M HCl at a 30 mg ml^{-1} concentration, with pepsin added at 1 mg ml^{-1} [22]. The mixture was stirred at 100 rpm for 48 h while maintained at 4 °C. Subsequently, the solution was neutralised to physiological pH using 10 M NaOH while keeping the temperature low. Furthermore, the neutralised dECM solution was reconstituted into a physiologically relevant buffered system by adding 10× PBS and sterile deionised water and stored at 4 °C before use.

2.15. Gelation of photo-crosslinked dECM hydrogels

For initial hydrogel formation, 1% (w/v) solubilised dECM generated from different decellularisation protocols was blended with Ru/SPS (0.5/5 mM) and exposed to visible light (30 mW cm^{-2}) for 3 min to induce crosslinking [20]. To examine mechanical tunability, hydrogels were generated using different Ru/SPS concentrations (1/10 and 2/20 mM). For crosslinking, 30 μl of each formulation was distributed into individual wells of a 24-well plate.

2.16. Microindentation test

The mechanical properties of cell-free hydrogel constructs were assessed using microindentation compression testing following overnight equilibration in PBS at 37 °C, as previously described [14, 34]. Measurements were performed using a piezoelectric actuator-driven microcompression system (MicroSquisher, CellScale Biomaterials Testing, Waterloo, Canada) maintained at 37 °C in a PBS bath (pH 7.4). Before testing, the indenter approached the hydrogel surface at a constant jogging speed of 4 μm s^{-1}. For each measurement, a dECM hydrogel sample was placed on the testing platform, and the indenter was aligned above the centre of the construct. Indentation was carried out using a 1 mm zirconium oxide bead (ZROB05, Next Advance, Troy, USA) attached to the end of a cantilevered steel microbeam with a diameter of 0.4064 mm. Cyclic compression was applied through the microbeam-bead assembly, generating vertical loading corresponding to 10% of the sample height. Each compression cycle consisted of a loading phase lasting 30 s, followed by a 30 s recovery phase, without an intermediate resting period. Three loading cycles were performed for each hydrogel specimen. During testing, the indentation force (F) and indentation depth (δ) were continuously determined from the optically measured deflection of the cantilever beam at the indenter tip together with the piezo-controlled z-displacement of the beam base. Changes in hydrogel thickness during compression were monitored, and the resulting force–displacement curves were recorded. The elastic modulus (E) of the hydrogel was subsequently calculated by fitting the force–indentation depth relationship to the Hertz contact model for a spherical indenter (equation (2)):

$$E = \frac{3\left(1-\nu^2\right)F}{4\,R^{0.5}\delta^{1.5}} \tag{2}$$

where R corresponds to the indenter radius, and ν represents Poisson's ratio of the material, taken as 0.44 [35, 36].

2.17. Swelling ratio and sol fraction

Immediately after visible-light crosslinking, the initial mass of each hydrogel (m_{initial}) was measured. The samples were subsequently frozen at −80 °C, freeze-dried, and weighed again to obtain the initial dry mass ($m_{initial\ dry}$). Following overnight equilibration in PBS at 37 °C, the hydrogels were gently blotted with laboratory wipes to remove excess buffer and weighed to determine the swollen mass ($m_{swollen}$). The samples were then lyophilised once more to obtain the final dry mass ($m_{final\ dry}$). The swelling ratio was calculated according to the equation shown below (equation (3)).

$$Swelling\ ratio\ (SR) = \frac{m_{swollen} - m_{initial\ dry}}{m_{initial\ dry}} \quad (3)$$

The sol fraction represents the portion of polymer chains that remain uncrosslinked within the network and was determined using equation (4) [37]:

$$Sol\ fraction = 100\% \times \frac{m_{initial\ dry} - m_{final\ dry}}{m_{initial\ dry}} \quad (4)$$

2.18. Rheology

The rheological behaviour of hydrogel precursor solutions was examined using a compact rheometer (MCR 302, Anton Paar, Graz, Austria) equipped with a Peltier-controlled plate for temperature regulation [14]. Shear rheology measurements were performed with a cone-plate geometry (CP25-1; 25 mm diameter, 1° cone angle, and a fixed gap of 0.05 mm). A solvent trap was not required because no sample drying occurred during testing, as verified beforehand. After positioning the measuring geometry and trimming the sample, a stabilisation period of 2 min was allowed to ensure mechanical and thermal equilibrium before data acquisition. Experiments were conducted under an H-ETD400 hood with the airflow switched off to minimise evaporation and maintain constant temperature conditions. Shear rate sweeps ranging from 0.1 to 1000 s^{-1} were applied to evaluate shear-thinning behaviour and viscosity. The rheological response of the hydrogel precursor solutions was further analysed by fitting the power-law model to the linear region of the shear rate-viscosity curves (equation (5)) [14].

$$\eta = K\dot{\gamma}^{n-1} \quad (5)$$

In this equation, η represents viscosity, $\dot{\gamma}$ denotes the shear rate, and K and n correspond to the shear-thinning coefficients.

2.19. Isolation and culture of hBMSCs

hBMSCs were isolated following a previously established protocol [38]. Bone marrow cell clusters were washed three times with PBS, finely minced, and incubated in RBC lysis buffer for 10 min at room temperature before centrifugation. The resulting cell pellet was resuspended in low-glucose DMEM supplemented with 10% FBS and 1% PS [39]. Cells were maintained in a humidified incubator at 37 °C with 5% CO_2 and passaged three times (P1–P3) once approximately 80% confluence was reached.

2.20. Cell encapsulation

hBMSCs were suspended in 1% cartilage dECM solution at a final density of 1×10^6 cells ml^{-1}. Aliquots of 30 μl of the hydrogel precursor mixture containing Ru/SPS were dispensed into individual wells of a 24-well plate and crosslinked as described previously. The resulting cell-laden constructs were cultured in 500 μl DMEM supplemented with 10% FBS and 1% PS in a humidified incubator at 37 °C with 5% CO_2, with medium replaced every two days.

2.21. Live/dead cell viability staining

Cell viability within the hydrogel constructs was assessed on days 1 and 7, using 1 μg ml^{-1} Calcein AM and PI. Briefly, cell-laden hydrogels were rinsed three times with PBS and incubated with the staining solution at 37 °C for 5 min. After staining, the constructs were washed three additional times with PBS and imaged using a fluorescent Zeiss microscope (Axio Imager M2, Carl Zeiss, Jena, Germany). Z-stack images were acquired with a step size of 10 μm over a total depth of 200 μm for each sample. Cell viability was quantified in ImageJ by separating the red and green fluorescence channels, applying threshold-based masks, and counting the corresponding particles. Viability was expressed as the percentage of live cells relative to the total number of cells.

2.22. PrestoBlue metabolic assay

Cellular metabolic activity was evaluated using the PrestoBlue assay. Following removal of the culture medium, each hydrogel was incubated with 500 μl of PrestoBlue reagent diluted 1:10 in pre-warmed medium at 37 °C for 2 h. After incubation, 100 μl of the resulting supernatant was collected and added in duplicate to a 96-well plate. Fluorescence intensity was measured using a CLARIOstar microplate reader (BMG Labtech, Ortenberg, Germany) with excitation at 540 nm and emission at 590 nm.

2.23. Chondrogenic differentiation

Passage 3 hBMSCs were harvested and suspended in dECM precursor solution containing Ru/SPS (0.5/5 mM) at a final density of 5×10^6 cells ml^{-1}. Aliquots of 30 μl of the hydrogel precursor mixture were dispensed into individual wells of a 24-well plate and crosslinked as described in section 2.15.

The resulting cell-laden constructs were cultured in chondrogenic medium consisting of high-glucose DMEM supplemented with 10 ng ml^{-1} TGF-β3, 100 nM dexamethasone, 50 μg ml^{-1} ascorbic acid 2-phosphate, 100 μg ml^{-1} sodium pyruvate, 40 μg ml^{-1} proline, and ITS-plus (final concentrations: 6.25 μg ml^{-1} insulin, 6.25 μg ml^{-1} transferrin, 6.25 ng ml^{-1} selenious acid, 5.33 μg ml^{-1} linoleic acid, and 1.25 mg ml^{-1} bovine serum albumin) [40]. Chondrogenic medium was replaced every two days. A 10% (w/v) GelMA was dissolved in PBS, mixed with hBMSCs at the same density, and subsequently crosslinked as described above.

2.24. Gene expression

Cell-laden hydrogels were rinsed three times with PBS and lysed with 1 ml TRIzol reagent for total RNA extraction according to the previously described protocol [41]. cDNA was generated using the High-Capacity cDNA Reverse Transcription Kit. Gene expression was then analysed using SYBR™ Green PCR Master Mix on a QuantStudio Real-Time PCR system (QuantStudio 6 Flex, Applied Biosystems, Waltham, USA). Primer sequences used for qRT-PCR are provided (supplementary table S1).

2.25. Fluorescence imaging

hBMSC-laden hydrogels were fixed in 4% PFA for 1 h and subsequently stored in PBS at 4 °C. The gels were then blocked overnight at 4 °C in blocking solution containing 5% (w/v) BSA and 0.1% (v/v) Triton X-100 in PBS [5]. Afterwards, samples were incubated with the primary antibody diluted in staining buffer (2% BSA in PBS, w/v) overnight at 4 °C, followed by three washes of 2 h each in the same buffer. The gels were subsequently incubated overnight at 4 °C with the secondary antibody, and DAPI was prepared in staining buffer. After three additional 2 h washes in staining buffer and a final PBS rinse, the samples were stored in PBS and imaged using an Evident FV4000 confocal microscope (Evident, Tokyo, Japan) equipped with a 20× objective. Details of the antibodies were listed in supplementary tables S2 and S3.

2.26. Image quantification

Z-stack images were converted into maximum-intensity projections using ImageJ. HIF-1α activation was then quantified by measuring fluorescence intensity normalised to DAPI, following previously established methods [42]. Image analysis parameters were defined using a particle size range of 50 μm to infinity and a circularity threshold of 0.3–1.

2.27. Oxygen-scavenging capsules seeding

Oxygen-scavenging capsules were supplied by collaborators and prepared as previously described [21]. In brief, the capsules consisted of semi-permeable, dopamine-coated structures encapsulating glucose oxidase (1000 U ml^{-1}) and catalase (60 000 U ml^{-1}). The stock suspension was provided in PBS at 500 mg ml^{-1} and subsequently diluted to final concentrations of 5–20 mg ml^{-1} in the hydrogel formulations.

2.28. Oxygen concentration measurements

Oxygen levels within the hydrogels were quantified as percentage air saturation using a PreSens oxygen profiling microsensor (PM-PSt7-02-L2.5-TS-NB40/0.8-NOP, PreSens GmbH, Regensburg, Germany) [16]. The microsensor was calibrated before use according to the manufacturer's instructions. All measurements were conducted at 37 °C under 5% CO_2 to match standard cell culture conditions. Before each reading, the sensor was held in position for 30 s to allow signal stabilisation. Measurements were collected on days 1 and 7.

2.29. RNA sequencing

Total RNA from the hBMSCs was extracted using TRIzol reagent, following the previously described protocol [41]. Small RNA cDNA libraries were generated using M-MLV Reverse Transcriptase (M1705, Promega, Madison, USA) and subjected to 50-nt single-end sequencing on the HiSeq 2500 platform (Illumina, San Diego, USA) [16]. Raw FASTQ files were processed with nf-core/smrnaseq (v3.18.0) [43] to generate miRNA counts against miRBase v22.1 [44]. Differential expression was analysed using DESeq2 with median-of-ratios normalisation [45], and significant miRNAs were defined as those with a false discovery rate (FDR) < 0.05 and $|\log_2 FC| \geqslant 1$ [46]. Functional enrichment analysis was carried out with clusterProfiler [47], including Kyoto Encyclopedia of Genes and Genomes (KEGG) pathways as well as gene ontology (GO) terms covering biological process, molecular function, and cellular component (CC), and gene set enrichment analysis (GSEA) v4.4.0 was used to test enrichment against MSigDB Hallmark pathways using $\log_2$ fold-change-ranked genes [48].

2.30. Statistical analysis

Statistical analyses were performed using GraphPad Prism v10. Data were obtained from at least three independent experiments and are presented as mean ± standard deviation (S.D.). Comparisons between two groups were conducted using Student's *t*-test with Welch's correction. For comparisons involving three or more groups, one-way ANOVA followed by Tukey's multiple-comparisons test was applied unless otherwise specified. Data normality was evaluated using the Shapiro–Wilk test, and grouped datasets were analysed by two-way ANOVA with Tukey's correction. Statistical significance was defined as $p < 0.05$, with $p < 0.05$, $p < 0.01$, $p < 0.001$, and $p < 0.0001$ indicated as *, **, ***, and ****, respectively.

3. Results

3.1. Detergent-mediated decellularisation strategies for bovine cartilage

Cartilage dECM suitable for further processing was generated through a stepwise decellularisation protocol involving detergent extraction, cryosectioning, lyophilisation, and enzymatic digestion (figure 1(a)). Hydrogel formation was qualitatively assessed using an inversion test following temperature-induced gelation, and the formed hydrogel appeared relatively clear under the present preparation conditions. Three decellularisation conditions were compared: 1% SDS, 2% SDS, and 1% Triton–0.1% NH_4OH. H&E staining revealed dense cellularity and well-preserved lacunar structure in native cartilage. In contrast, all decellularisation groups showed near-complete nuclear removal (figure 1(b)). SDS-based treatments produced more extensive matrix expansion and fibre loosening, particularly under 2% SDS, indicative of marked detergent-mediated ECM disruption [49]. The 1% Triton–0.1% NH_4OH protocol yielded the most uniform ECM preservation, with minimal structural distortion observed across both magnifications. Further confirmation of removal in decellularised tissues was obtained via DAPI staining (supplementary figure S1). GAGs, primarily chondroitin and keratan sulphate, are major components of aggrecan in articular cartilage [50]. Safranin-O staining showed the expected intense signal for GAGs in native tissue (figure 1(c)). Treatment with 1% or 2% SDS resulted in a pronounced GAGs depletion, reflected by reduced staining intensity and heterogeneous surface loss. Semi-quantification of the Safranin-O-positive area further confirmed reduced GAGs retention in the SDS-treated groups, while the 1% Triton–0.1% NH_4OH group remained comparable to native tissue (figure 1(d)). Notably, the 1% Triton–0.1% NH_4OH group retained substantially more Safranin-O signal, indicating superior preservation of sulphated GAGs compared to SDS groups. Quantitative DNA analysis confirmed the histological findings (figure 1(e)). Native cartilage contained high DNA levels, whereas all decellularised samples showed significant reductions ($p < 0.0001$). SDS-based protocols achieved the most complete removal, approaching near-background levels. The 1% Triton–0.1% NH_4OH method also significantly reduced DNA content relative to native tissue, although residual amounts were slightly higher than in SDS-treated groups. All decellularisation methods achieved significant dsDNA removal (85%–95%) compared with native tissue, consistent with previous reports and critical for minimising the immunogenicity associated with residual DNA [23]. GAG quantification revealed a marked reduction following SDS treatment (figure 1(f)). Both the 1% SDS and 2% SDS groups exhibited significantly lower GAG content compared with native cartilage ($p < 0.0001$). In contrast, the 1% Triton–0.1% NH_4OH method preserved GAGs at levels not significantly different from native tissue, aligning with the Safranin-O staining patterns and supporting the conclusion that milder decellularisation conditions result in superior ECM retention.

The biochemical composition and mechanical environment provided by cartilage ECM are important determinants of cellular responses [51, 52]. Picrosirius red staining under PLM was employed to visualise the collagen network after decellularisation. Tissues treated with 1% Triton–0.1% NH_4OH exhibited green birefringence, resembling native cartilage tissue (supplementary figure S2(a)) [53]. In contrast, SDS-treated tissues showed predominant yellow-red birefringence, likely due to SDS-induced disruption of collagen's macromolecular structure [23, 49, 54]. SEM analysis showed that the overall microfibrillar architecture of the collagen network remained relatively intact across all conditions (supplementary figure S2(b)). Taken together, this discrepancy likely arises because PLM detects subtle SDS-induced changes in collagen molecular structure and birefringence that do not translate into obvious alterations of fibrillar morphology by SEM [55]. Biochemical composition was assessed by FTIR, with collagen and proteoglycan distributions inferred from the amide I (1720–1590 cm^{-1}) and carbohydrate (1140–985 cm^{-1}) peaks, respectively (supplementary figure S2(c)) [56]. Spectra from 1% Triton–0.1% NH_4OH–treated samples closely resembled native cartilage with preserved collagen and proteoglycan, whereas SDS-treated tissues showed reduced absorbance (supplementary figure S2(c)), consistent with decreased GAG content (figure 1(f)). Furthermore, nanoindentation testing (supplementary figure S2(d)) revealed no significant differences in mechanical properties between native cartilage and any of the dECM tissues. Overall, 1% Triton–0.1% NH_4OH demonstrated superior preservation of ECM components.

3.2. Protein identification and functional enrichment of decellularised cartilage tissue

The protein composition of the dECMs was analysed by mass spectrometry and compared with native bovine cartilage [23]. Pairwise comparison identified 407, 507, and 411 DEPs in the 1% SDS, 2% SDS, and 1% Triton–0.1% NH_4OH conditions, respectively ($|\log_2 FC| \geqslant 0.5$ and $p \leqslant 0.05$) (figure 2(a)). Notably, the 1% Triton–0.1% NH_4OH-treated dECM exhibited the highest number of upregulated proteins (188) and the fewest downregulated proteins (212), indicating better preservation of the native proteome than the SDS-based methods (figure 2(a)). The proportion of matrisome and non-matrisome DEPs under each decellularisation condition was determined by comparison to the matrisome database of ECM and ECM-associated proteins [57] (figure 2(b)). Among all groups, the 1% Triton–0.1% NH_4OH-treated dECM demonstrated the highest matrisome

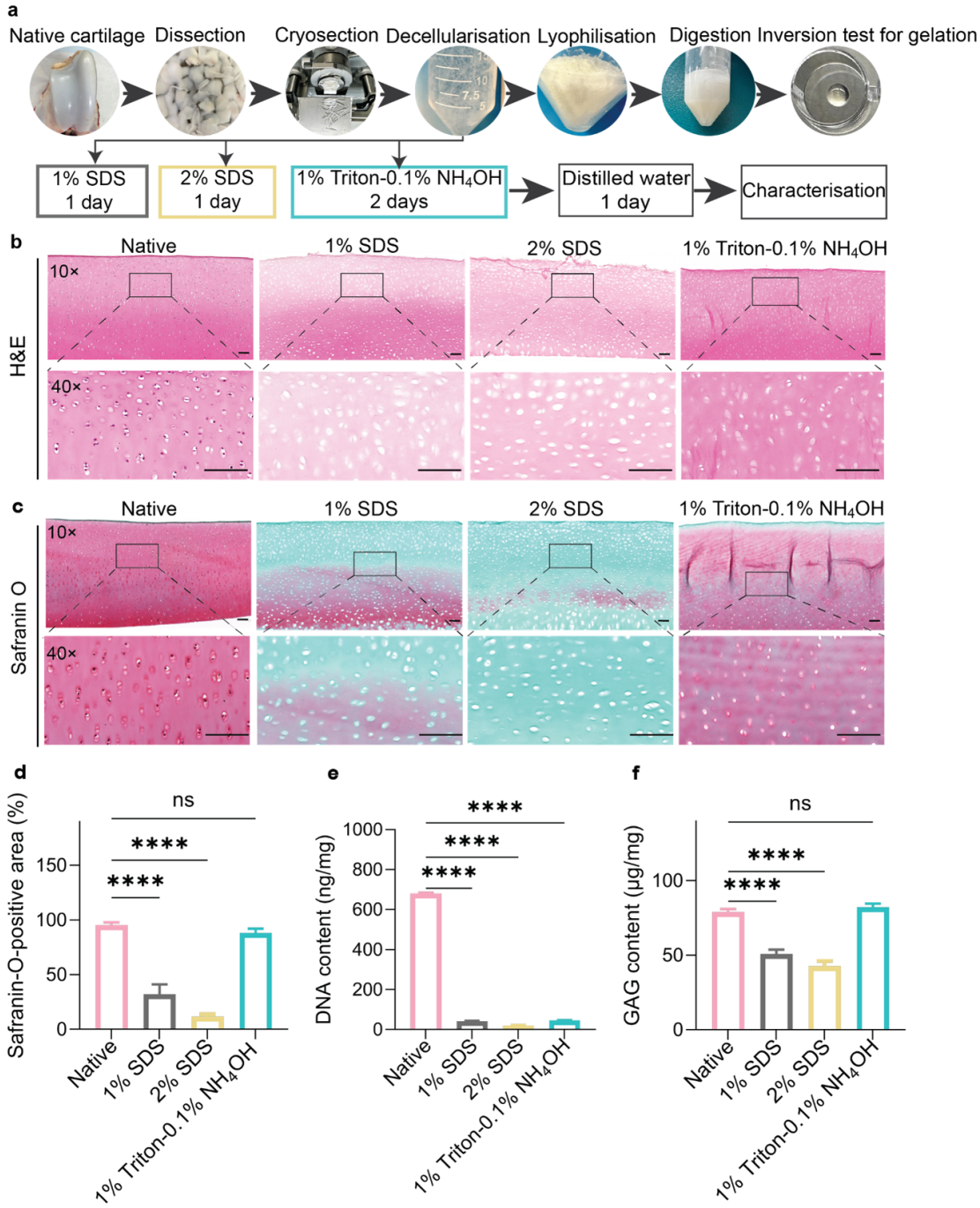

Figure 1. Decellularisation of bovine cartilage. (a) Schematic overview of the decellularisation process. (b) Hematoxylin and eosin (H&E) staining of native and decellularised cartilage for different detergent conditions. The insets in the upper panels are shown at higher magnification in the lower panels. Scale bar = 100 μm. (c) Safranin O staining of native and decellularised cartilage. Scale bar = 100 μm. (d) Semi-quantification analysis of Safranin-O-positive area (%). (e) DNA content of bovine cartilage throughout the decellularisation process, normalised to dry weight. (f) Glycosaminoglycan (GAG) content in native and decellularised bovine cartilage, normalised to dry weight. Representative images are shown in (b) and (c), with one representative image shown for each group ($n = 3$ bovine cartilage samples). Data in (d) are presented as mean ± S.D. ($n = 3$ bovine cartilage samples per group, with 3 technical replicates per sample). Data in (e) and (f) are presented as mean ± S.D. ($n = 3$ bovine cartilage samples).

content (23%) and the most significant proportion of upregulated matrisome proteins (66%), compared with 17% and 20% for 1% SDS and 18% and 45% for 2% SDS (figure 2(b)). The predominant matrisome components identified in all dECMs are core matrisome proteins, including ECM glycoproteins, proteoglycans, and collagens, which are essential for maintaining the mechanical properties and regulating [58]. Notably, 1% Triton–0.1% NH_4OH treatment resulted in the highest upregulation of ECM glycoproteins (67%) and proteoglycans (50%), compared with 37% and 7% for 1% SDS and 26% and 0% for 2% SDS conditions (figure 2(c)). Collagen remained comparable across groups at 11%, 8%, and

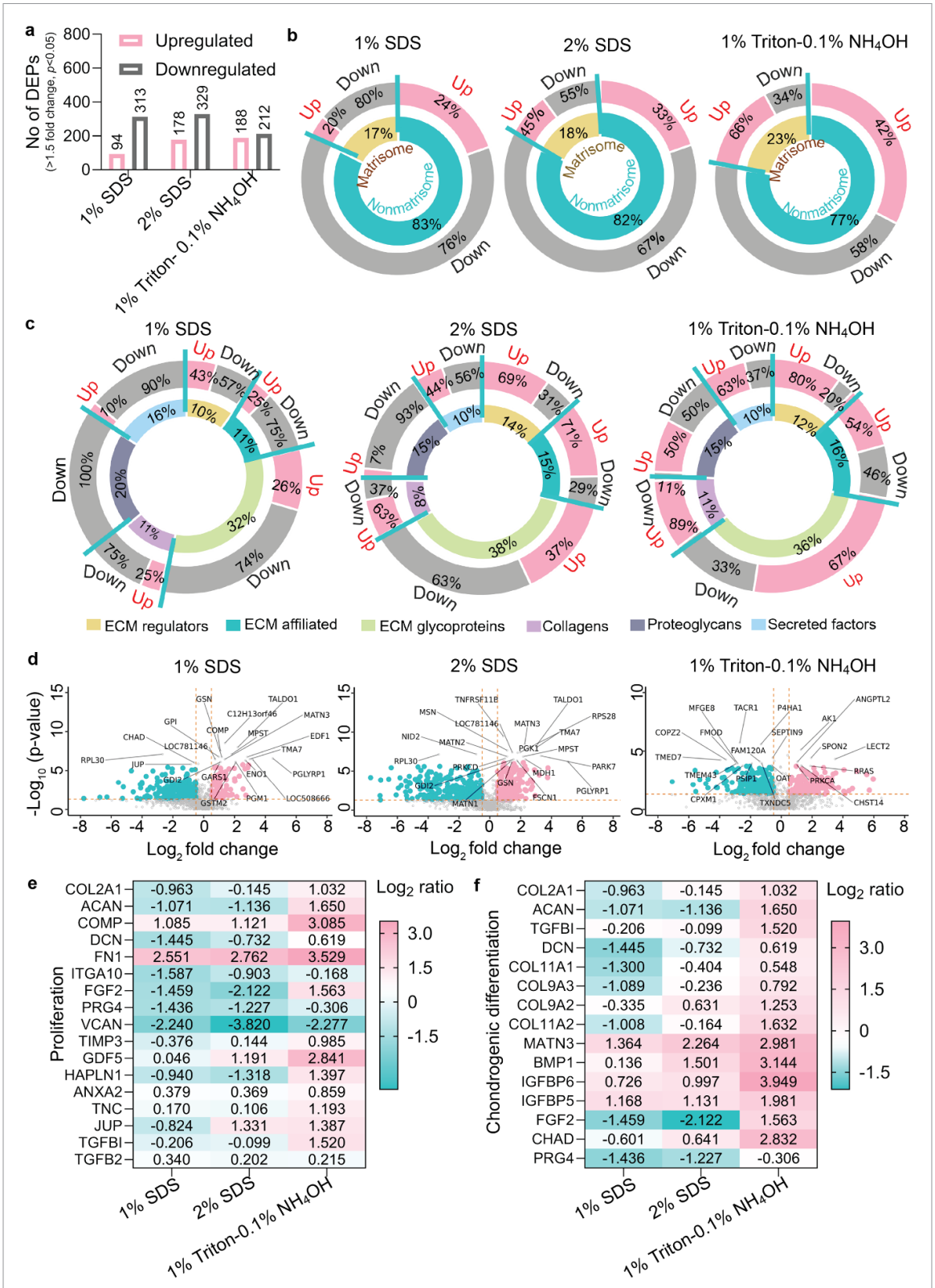

Figure 2. Proteomic analysis of decellularised extracellular matrix (dECM) generated from each decellularisation condition relative to native bovine cartilage. (a) Number of differentially expressed proteins (DEPs) upregulated and downregulated in different decellularised cartilage dECMs compared to the native cartilage. (b) Matrisome and non-matrisome proteins in dECMs relative to the native cartilage. (c) Subtypes of matrisome proteins in dECMs compared to native cartilage. (d) Volcano plot depicting the total protein expression in dECMs relative to that in native cartilage. Red dots indicate significantly upregulated proteins, and blue dots indicate significantly downregulated proteins ($|\log_2$ fold change (FC)$| \geqslant 0.5$ and $p \leqslant 0.05$). (e), (f) Heatmaps showing the $\log_2$ ratio for chondrocyte proliferation-related proteins (e) and articular chondrogenic differentiation-related proteins (f) in each group relative to native cartilage. All data were obtained from $n = 3$ bovine cartilage samples per group.

11% for 1% SDS, 2% SDS, and 1% Triton–0.1% NH_4OH, respectively (figure 2(c)).

We next compared the protein profiles between native cartilage and each dECM using the volcano plot ($|\log_2 FC| \geqslant 0.5$, $p \leqslant 0.05$), highlighting the top 20 DEPs (figure 2(d)). In the 1% SDS and 2% SDS groups, 17 and 18 proteins were upregulated, respectively, mainly non-matrisome proteins [59], with only 3 and 2 proteins downregulated, including the matrisome proteins CHAD and NID2 (figure 2(d)). In contrast, the 1% Triton–0.1% NH_4OH-treated dECM showed more extensive downregulation, largely of non-matrisome proteins, suggesting more efficient removal of cellular and immune-related proteins while relatively preserving structural matrix components (figure 2(d)).

To further assess whether decellularisation altered proteins regulating cell proliferation and chondrogenic differentiation, we queried the NCBI Gene database and literature to compile a curated list (supplementary table S4) of proteins linked to chondrocyte proliferation and articular chondrogenic differentiation [60–70] and to map those onto our dECM proteomic data. This analysis showed that the 1% Triton–0.1% NH_4OH-treated dECM was enriched in proteins promoting chondrocyte proliferation (e.g. TGF-β1, COMP, FN, DCN, PRG4) and chondrogenic differentiation (e.g. COL2A1, ACAN, PRG4, TGF-β1) (figures 2(e) and (f)). Building upon these findings, pathway enrichment and upstream regulator analyses were also performed to elucidate the molecular mechanisms underlying the differential protein expression among the decellularisation conditions. Analysis of the top 20 canonical pathways revealed that proteins involved in cell survival, proliferation, and differentiation were consistently higher in the 1% Triton–0.1% NH_4OH-treated dECM than in either SDS-treated group, particularly extracellular matrix organisation and interleukin-4 (IL-4) signalling, both critical for chondroprotection and tissue regeneration (supplementary figure S3) [60–62]. Upstream regulator analysis further confirmed that the 1% Triton–0.1% NH_4OH-treated dECM enriched proliferation-related proteins (TGF-β1, TGF-β3, IGF-1, DCN) and differentiation-related proteins (TGF-β1, TGF-β3, TGF-βR1, SOX9) (supplementary figures S4(a) and (b)). Overall, these data suggest that this decellularisation protocol efficiently removes nuclear material while preserving native proteins that support chondrocyte proliferation and chondrogenic differentiation toward an articular phenotype.

3.3. Formation and characterisation of cartilage dECM hydrogels and biocompatibility assessment

Cartilage-derived dECM from all experimental conditions was solubilised by pepsin digestion in 0.1 M HCl for 48 h to prepare the prepolymer solution for visible-light-induced crosslinking using the Ru/SPS system (figure 3(a)). Upon visible-light exposure (400–450 nm), Ru/SPS generates tyrosyl radicals that form covalent dityrosine bonds between adjacent tyrosine residues, establishing the hydrogel network [6]. Tyrosine, abundant in collagen, the main structural protein in dECM, facilitates both protein conformational stabilisation and photo-crosslinking [71]. Following the addition of Ru/SPS (0.5/5 mM), all dECM solutions rapidly formed translucent yellow spherical hydrogels under visible light (figure 3(b)). Unlike conventional thermally assembled dECM hydrogels, network formation was achieved through photo-initiated crosslinking [22]. Rheological analysis further showed that all dECM prepolymer solutions exhibited non-Newtonian, shear-thinning behaviour over a shear rate of 0.1–1000 s^{-1} range (figure 3(c)), a key property for extrusion-based biofabrication that minimises cell damage while maintaining structural fidelity [72].

We next assessed sol fraction and swelling ratio to evaluate the physicochemical properties of the photo-crosslinked dECM hydrogels (figures 3(d) and (e)). The 1% Triton–0.1% NH_4OH group indicated the lowest sol fraction, consistent with its reduced swelling ratio, which suggests a higher crosslinking density than the SDS-treated dECM gels. Mechanical testing by microindentation revealed that all photo-crosslinked hydrogels were markedly stiffer than conventional thermally crosslinked dECM hydrogels (0.002–1 kPa) reported previously [7, 22], with the 1% Triton–0.1% NH_4OH condition exhibiting the highest compressive Young's modulus (12.87 ± 2.13 kPa) (figure 3(f)). This enhanced stiffness is likely attributable to dityrosine crosslinking formation under visible light, which increases resistance to mechanical stress and improves shape fidelity.

Photo-crosslinked hydrogels obtained from each decellularisation protocol were further examined for their cytocompatibility. hBMSCs were encapsulated within 1% dECM mixed with 0.5/5 mM Ru/SPS and crosslinked under visible light (30 mW cm^{-2}) for 3 min, followed by live/dead staining on days 1 and 7 (figure 3(g)) and cell viability assays at 24 h (figure 3(h)). Hydrogels derived from 1% Triton–0.1% NH_4OH-reated dECM were cytocompatible, whereas both SDS-derived hydrogels were cytotoxic, likely due to residual SDS, consistent with previous studies [73, 74]. Proliferation-related gene expression (*MCM2*, *Ki67*, *CDK1*, *PCNA*, and *Cyclin D1*) was also increased in hBMSCs cultured in 1% Triton–0.1% NH_4OH-treated dECM hydrogels at day 7 relative to day 1 (supplementary figure S5), and this condition was therefore selected for all subsequent experiments.

Having established 1% Triton–0.1% NH_4OH as the decellularisation condition, we next examined the effect of Ru/SPS concentration on hydrogel mechanics and cell behaviour. Increasing the concentration of Ru/SPS elevated the Young's modulus (12.9–33.3 kPa) (supplementary figure S6), but

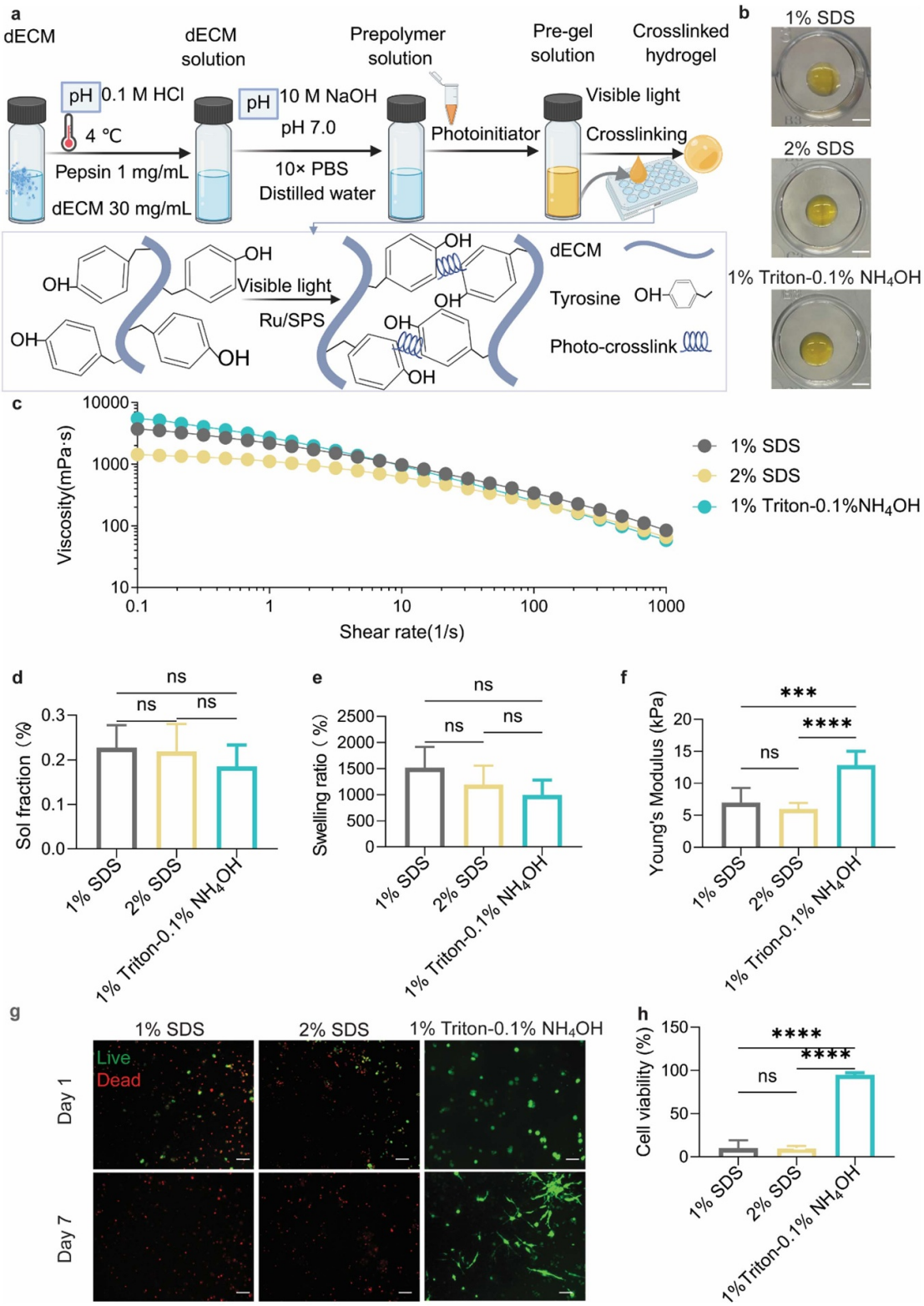

Figure 3. Solubilisation and tyrosine-based light-activated crosslinking reaction in dECM pregel solution and evaluation of biocompatibility. (a) A schematic of pepsin-mediated solubilisation and visible light-activated dityrosine formation. (b) Photographs of photo-crosslinked dECM hydrogels generated from each decellularisation condition. Scale bar = 2.5 mm. One representative photograph is shown for each group. (c) Rheological properties of dECM pregel solutions measured by rheometer. One representative dataset is shown for each group ($n = 4$ pregel solution samples). (d) Sol fraction. (e) Swelling ratio. (f) Young's modulus in compression quantified by microindentation. (d)–(f) are presented as mean ± S.D. ($n = 6$ hydrogel samples per group). (g) Live (Calcein AM)/dead (Propidium iodide (PI)) staining of human bone marrow-derived mesenchymal stem cells (hBMSCs) cultured in dECM hydrogels in all conditions for 1 and 7 d. Scale bar = 100 μm. One representative image is shown per group ($n = 3$ hydrogel samples). (h) Quantification of cell viability (percentage of live cells relative to total cells) on day 1 of culture. Data are presented as mean ± S.D. ($n = 3$ hydrogels analysed with $n = 3$ technical replicates).

reduced hBMSCs proliferation and metabolic activity within dECM hydrogels (supplementary figures S7(a) and (b)), likely associated with excessive free radical generation from higher photoinitiator levels [75].

3.4. Evaluation of chondrogenic capability of photo-crosslinked dECM hydrogels

The *in vitro* chondrogenic induction capacity of scaffolds is critical for effective articular cartilage regeneration. To evaluate the ability of cartilage dECM hydrogels to support the articular cartilage-specific functions of hBMSC-derived chondrocytes, we used 1% dECM combined with 0.5/5 mM Ru/SPS and compared its performance to 10% GelMA, a widely used benchmark in cartilage regeneration and tissue engineering [76].

By day 21, hBMSC-derived chondrocytes in dECM hydrogels exhibited a markedly higher expression of chondrogenic genes than those in GelMA (figure 4(a)). *SOX9*, a key transcription factor driving chondrogenic and regulating matrix genes, such as *ACAN* and *COL2A1* [77], was significantly upregulated in dECM hydrogels. Notably, *COL2A1* expression increased 28-fold ($p < 0.0001$) in dECM versus 9-fold in GelMA, and ACAN expression was also elevated. In contrast, *COL1A1* levels remained unchanged in GelMA and were slightly reduced in dECM. Given that *COL2A1* is a characteristic of hyaline articular cartilage and *COL1A1* is associated with fibrocartilage [78], the *COL2*/*COL1* ratio serves as a key indicator of a chondrogenic phenotype. This ratio was significantly higher in dECM, although still below 1 (figure 4(b)). Consistently, immunostaining revealed a more extensive distribution of COL2A1 in dECM hydrogels (figure 4(c)). Together, these results indicated that cartilage-derived dECM hydrogels promote and maintain an articular-like chondrogenic phenotype.

3.5. Photo-crosslinking-compatible oxygen-scavenging microcapsules enhance hBMSC chondrogenesis

Hypoxia (1%–5%) is known to enhance the stemness and chondrogenic potential of mesenchymal stem cells (MSCs), better reflecting the native niche of progenitor cells and articular chondrocytes [79]. In addition to embedding cells, bioink can be supplemented with oxygen-scavenging components to locally reduce the oxygen level. However, this may be incompatible with Ru/SPS-based photo-crosslinking, which relies on oxygen-driven photo-oxidation of phenol-modified polymers and is markedly impaired under anaerobic conditions [17, 18]. Herein, we investigate whether integrating the oxygen-scavenging microcapsules [21] into cartilage dECM affects photo-crosslinking and, in turn, facilitates a hypoxic microenvironment that enhances chondrogenic differentiation of hBMSCs.

Oxygen-scavenging microcapsules loaded with glucose oxidase and catalase are dispersed throughout the hBMSC-laden cartilage dECM hydrogel (figure 5(a)). Glucose oxidase converts glucose and dissolved O_2 into gluconic acid and H_2O_2, while catalase rapidly decomposes H_2O_2, leading to a net consumption of oxygen and the formation of a localised hypoxic niche surrounding the cells. We first evaluated the photo-crosslinking behaviour of cartilage dECM hydrogels containing 5, 10, and 20 mg ml^{-1} oxygen-scavenging microcapsules to ensure that their incorporation did not disrupt Ru/SPS-mediated crosslinking (supplementary figure S8). Notably, 20 mg ml^{-1} has previously been reported to lower oxygen concentration to ∼2% within 2 h in GelMA [21]. After confirming structural integrity, we quantified the oxygen levels in hBMSC-laden constructs cultured in a conventional 37 °C, 5% CO_2 cell culture incubator on days 1 and 7 (figure 5(b)), observing that cell-only hydrogels remained normoxic (∼18% on day 7), whereas microcapsule-loaded hydrogels reached hypoxic conditions of 7.5%, 3.7%, and 3.2% for 5, 10, and 20 mg ml^{-1}, respectively (figure 5(b)), consistent with the reported month-long scavenging stability of these capsules [21]. We then examined the viability of hBMSCs under microcapsule-mediated hypoxia and found no significant differences in live/dead staining among hydrogels containing 5, 10, or 20 mg ml^{-1} microcapsules on days 1 and 7 (figure 5(c), supplementary figures S9(a) and (b)). Given the minimal difference between the 3.7% and 3.2% O_2, 10 mg ml^{-1} was selected as the concentration for inducing hypoxia in subsequent chondrogenic differentiation experiments.

We assessed the cellular response to microcapsule-induced hypoxia within the hydrogel system by examining hypoxia-inducible factor 1α (HIF-1α), a key oxygen-sensitive transcription factor. hBMSCs cultured in hypoxic dECM hydrogels containing oxygen-scavenging microcapsules under a standard incubator (20% O_2) showed strong nuclear localisation of HIF-1α, indicating activation of the hypoxic signalling, whereas cells in normoxic hydrogels without microcapsules exhibited weak diffuse HIF-1α (figures 5(d) and (e)). These results, in line with the previous report, confirm that oxygen-scavenging microcapsules can effectively induce a hypoxic response *in vitro* without the need for a dedicated hypoxia incubator [21]. To investigate how oxygen tension shapes the phenotype of hBMSC-derived chondrocytes, hBMSCs were differentiated in either hypoxic or normoxic dECM hydrogels. Consistent with the previous study, which found that hypoxia enhances hBMSCs chondrogenesis [80], 14 days of hypoxia culture significantly upregulated COL2A1, ACAN, and SOX9, while markedly downregulating COL1A1 (figure 5(f)). The increased COL2A1 expression is

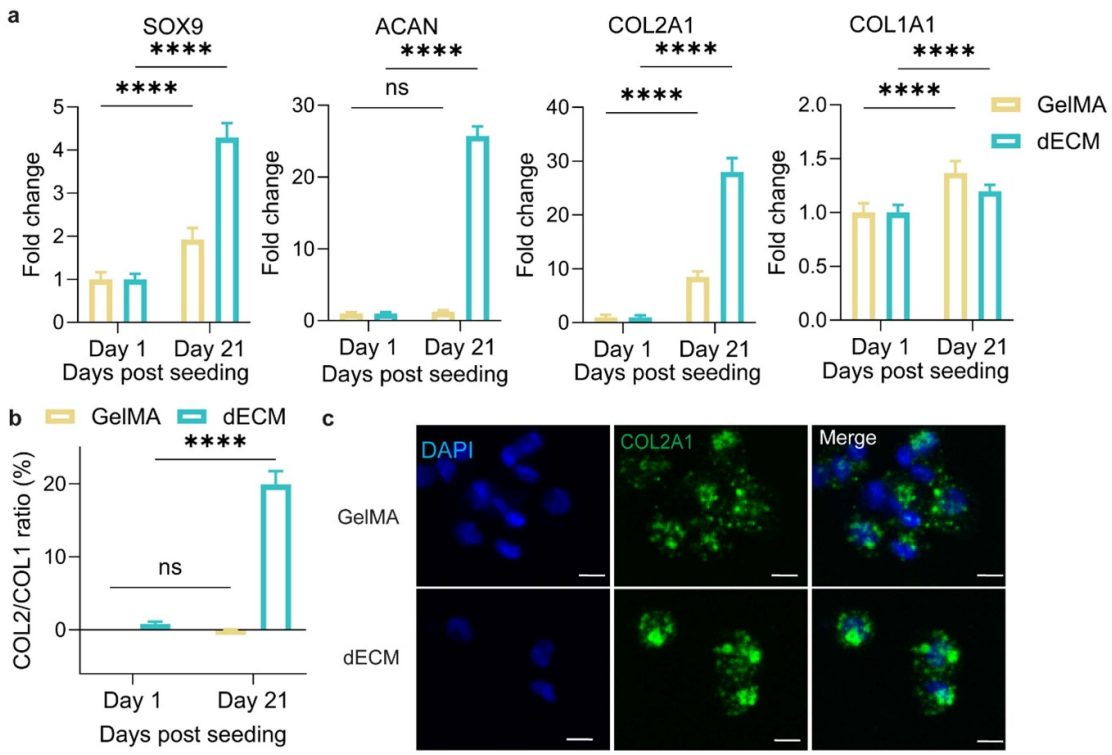

Figure 4. Evaluation of chondrogenic potential in photo-crosslinked dECM hydrogels. (a) Gene expression in hBMSC-derived chondrocytes after 21 d of chondrogenic differentiation. (b) Quantitative comparison of *COL2*/*COL1* ratio in hBMSC-derived chondrocytes after 21 d of chondrogenic differentiation. Data in (a) and (b) are presented as mean ± S.D. ($n = 3$ hydrogels analysed with $n = 3$ technical replicates). (c) Representative immunofluorescence images of COL2A1 staining in hBMSC-derived chondrocytes with DAPI after 21 d of chondrogenic differentiation. Scale bar = 5 μm. One representative image is shown for each group ($n = 3$ hydrogel samples).

likely mediated by HIF-1α-driven type II collagen synthesis [81]. Taken together, these findings showed that incorporating oxygen-scavenging microcapsules into photo-crosslinked cartilage-dECM hydrogels promotes the differentiation of hBMSC-derived chondrocytes toward a phenotype that better mimics the naturally hypoxic cartilage environment.

Given these phenotypic and marker changes, we next performed RNA sequencing on hBMSC-derived chondrocytes cultured in hypoxic versus normoxic dECM hydrogels to define the underlying transcriptional landscape. A total of 2,379 differentially expressed genes (DEGs) were identified ($|\log_2 FC| \geqslant 1$, FDR < 0.05), with many cartilage ECM-related genes prominently represented in the volcano plot (figure 6(a)). DEGs were mainly associated with cartilage matrix synthesis/organisation, signalling, and transcriptional regulation that supports a cartilage-producing, non-hypertrophic phenotype (figure 6(b)), a pattern further corroborated by the top 25 upregulated and downregulated genes (supplementary figures S10(a) and (b)), indicating increased cartilage ECM- and hypoxia-responsive transcription and reduced ECM remodelling and proliferation under hypoxia.

Functional enrichment analysis based on GO terms linked to collagen-containing extracellular matrix organisation and connective tissue development under hypoxic conditions (supplementary figure S11), suggesting a matrix-producing cartilage-like phenotype (figure 5(e)). To further confirm the impact of oxygen-regulated DEGs, genes associated with chondrocyte phenotype, hypoxia signalling, and metabolism were curated from the NCBI Gene database (supplementary table S5) [77, 82–88]. hBMSCs cultured in hypoxic cartilage dECM hydrogels showed upregulation of articular chondrocyte markers and cartilage-associated genes, including *COMP*, *PRG4*, *SOX5*, *SOX6*, *SOX9*, *SMAD2/3*, and *HAPLN1* (figure 6(c)), while hypertrophic markers such as *MMP13*, *SPP1*, *BMP2*, and *SP7* were suppressed (figure 6(d)). Canonical HIF target genes and metabolic effectors (*VEGFA*, *EPAS1*, *SC2A1*, *SLC2A3*, and *LDHA)* were strongly induced at 3% O_2, indicating robust hypoxic signalling and enhanced glycolysis (figure 6(e)). In addition, anabolic regulators (*TGF-β*, *IGF1/2*, and *FGFR3*) were upregulated (supplementary figure S12(a)), whereas catabolic regulators (e.g. *MMP13*, *ADMTS4*) were downregulated (supplementary figure S12(b)), supporting a non-hypertrophic cartilage phenotype in hBMSC-derived chondrocytes [16]. Hypoxia reprogrammed hBMSC-derived chondrocytes at both phenotypic and metabolic levels,

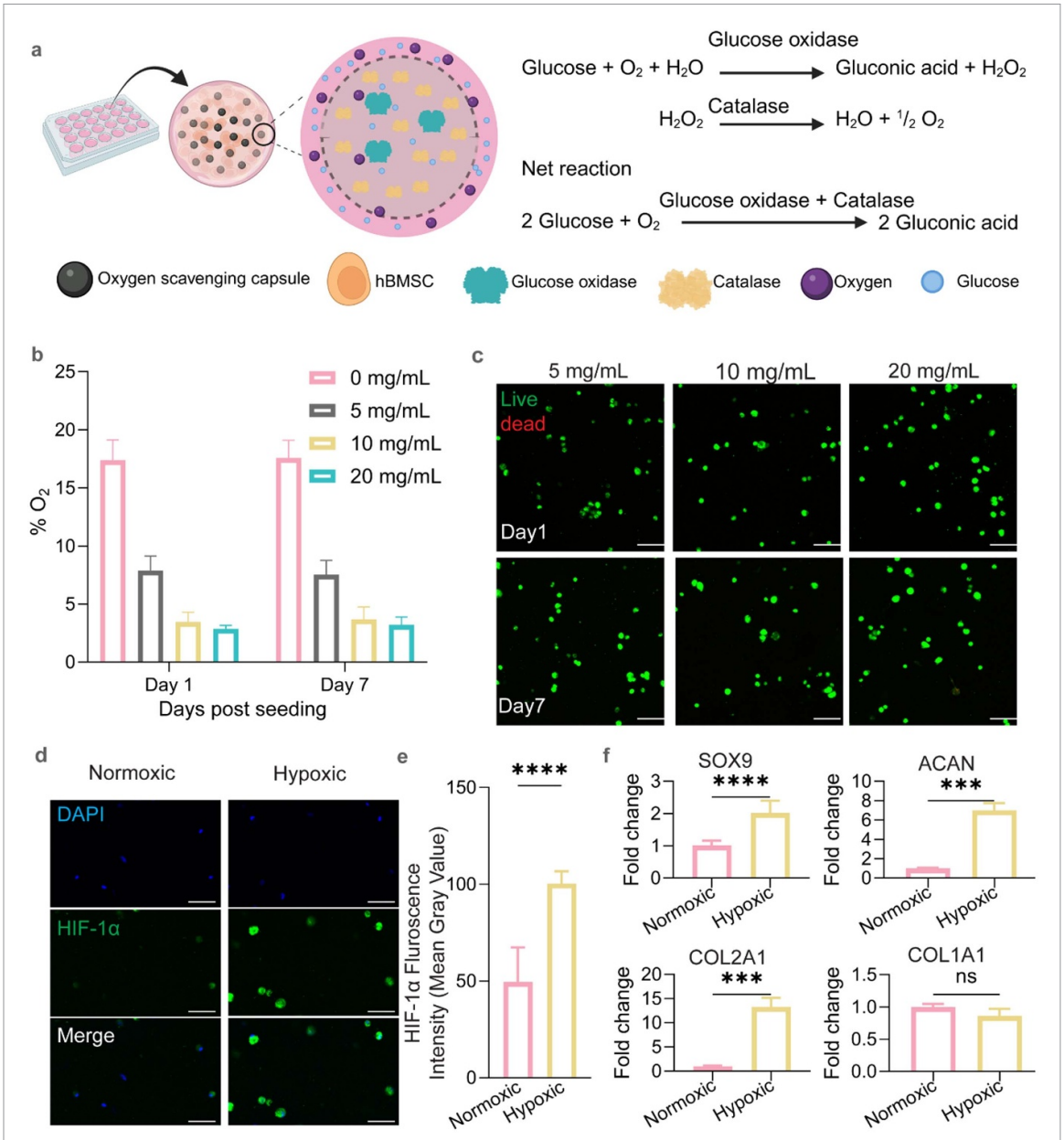

Figure 5. Oxygen-scavenging microcapsules enhancing the chondrogenic differentiation of hBMSCs. (a) Schematic of oxygen-scavenging microcapsules encapsulating glucose oxidase and catalase. (b) Oxygen levels in cartilage dECM hydrogels containing different concentrations of oxygen-scavenging microcapsules. Data are presented as mean ± S.D. ($n = 4$ hydrogel samples, each with $n = 3$ technical replicates). (c) Representative live (Calcein AM)/dead (PI) staining images of hBMSCs encapsulated in cartilage dECM hydrogels supplemented with different concentrations of oxygen-scavenging microcapsules after 1 and 7 d. Scale bar = 100 μm. One representative image is shown for each group ($n = 3$ hydrogels). (d) HIF-1α expression on day 7 of hBMSCs. Scale bar = 50 μm. One representative image is shown for each group ($n = 3$ hydrogels). (e) Quantification of HIF-1α expression. (f) Gene expression in hBMSC-derived chondrocytes after 14 d of chondrogenic differentiation. Data in (e) and (f) are presented as mean ± S.D. ($n = 3$ hydrogel samples, each with $n = 3$ technical replicates).

together with upregulated expression of genes associated with TGF-β/SMAD2/3 and IGF-1/2-IGF1R signalling, pathways associated with enhanced chondrogenesis and reduced hypertrophic differentiation [89, 90].

GSEA indicated downregulation of the Hedgehog signalling pathway, which is involved in chondrocyte hypertrophy and endochondral ossification. Reduced TNF-α/NF-κB signalling was also observed. This pathway promotes matrix degradation through matrix metalloproteinases (MMPs) and a disintegrin and metalloproteinase with thrombospondin motifs (ADAMTS) while suppressing extracellular matrix synthesis (figure 6(f)) [91, 92]. In contrast, glycolytic pathways were markedly enriched, consistent with the induction of canonical HIF target genes (*SLC2A1*, *SLC2A3*, *LDHA*, *BNIP3*, *EPAS1*, and *VEGFA*), indicating a HIF-dependent metabolic adaptation to hypoxia (figure 6(f)) [93]. The phosphoinositide 3-kinase (PI3K)-AKT-mechanistic target of rapamycin (mTOR) (PI3K-AKT-mTOR) pathway, which can promote chondrocyte proliferation

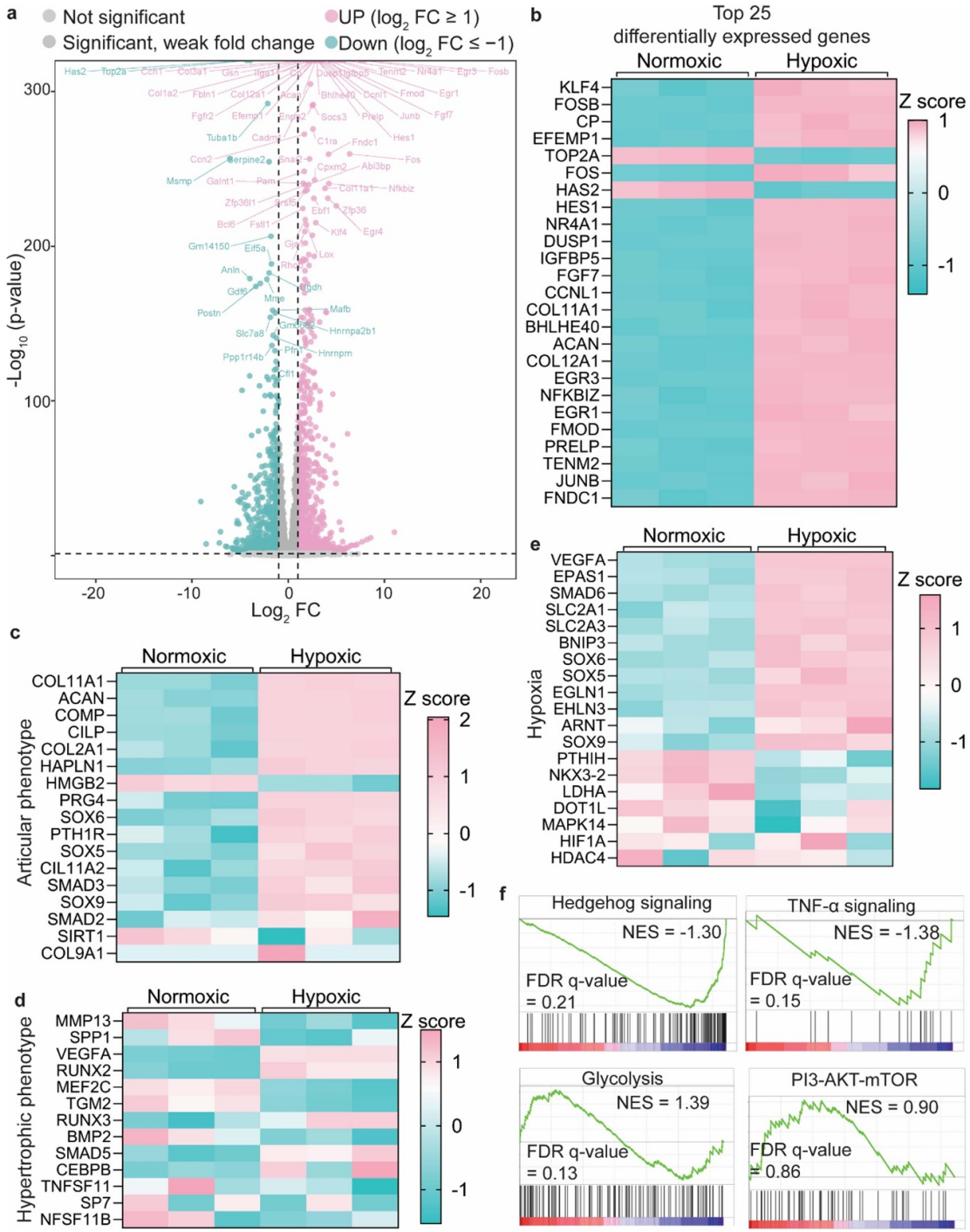

Figure 6. RNA-sequencing analysis of differentially expressed genes (DEGs) in hBMSC-derived chondrocytes cultured in photo-crosslinked dECM hydrogels under hypoxic (3% O_2) or normoxic (20% O_2) conditions. (a) Volcano plot showing DEGs between hypoxia and normoxia. $|\log_2 FC| \geqslant 1$, FDR < 0.05. (b) Heatmap of the top 25 DEGs. (c)–(e) Heatmaps of selected DEGs associated with articular chondrocyte phenotype (c), hypertrophic chondrocyte phenotype (d), and hypoxia-responsive genes (e). (f) Gene set enrichment analysis (GSEA) showing enrichment of Hallmark pathways associated with glycolysis, PI3K–AKT–mTOR signalling, TNF-α signalling, and Hedgehog signalling. RNA sequencing analyses were performed using $n = 3$ hydrogel samples per group. Gene sets with FDR < 0.25 were considered significantly enriched.

and matrix synthesis, showed minimal differences between normoxic and hypoxic conditions (figure 6(f)) [94]. Overall, these findings indicate that hypoxia primarily promotes metabolic reprogramming while suppressing inflammatory and hypertrophy-associated signalling in hBMSC-derived chondrocytes.

4. Discussion

dECM is regarded as a physiological reservoir of bioactive signalling molecules, as it preserves most of the functional and structural components of the native ECM [95]. When applied, these retained bioactive cues provide an inherent microenvironmental

niche that strengthens cell-matrix interactions, directs tissue- and organ-specific differentiation, and helps restore original cellular functions, making dECM a highly promising biomaterial for tissue engineering, disease modelling, and drug screening [96]. However, its broader application is limited by batch-to-batch variability, potential reduction of bioactivity during processing, and difficulties in large-scale standardisation [97]. A significant source of this variation is the lack of standardised decellularisation protocols across laboratories, resulting in notable differences in ECM composition and functional performance. For example, in cartilage-derived dECM, reported GAG retention ranges from 2% to 87% [98–101]. Because effective decellularisation is tissue-dependent, protocols must be carefully optimised for each tissue source and application. Herein, our work provides new data on how decellularisation conditions critically shape dECM compositions.

Three detergent-based decellularisation protocols were examined, revealing notable variations in the resulting dECM compositions, especially at the proteomic level. Detergent-based decellularisation methods were selected due to their reported efficiency and ease of implementation in previous studies [102]. SDS is an ionic detergent recognised for its ability to disrupt cell membranes and solubilise cellular debris [23]. Triton X-100 disrupts lipid-lipid and lipid-protein interactions in cellular membranes but largely spares protein-protein interactions, thereby solubilising cell membranes and organelles while leaving the ECM protein network relatively intact [103]. Although Triton X-100 alone showed good ECM preservation in cartilage, it is less effective in DNA removal [78]. The addition of NH_4OH, a charged base, appears to enhance its decellularisation efficiency [5], likely by increasing pH levels that promote nuclear lysis and solubilisation of nucleic proteins and DNA-protein complexes [14]. The 1% and 2% SDS protocols showed strong DNA removal performance. However, these conditions also caused substantial GAG reduction and cytotoxicity in hBMSCs, consistent with previous findings that SDS treatment leads to pronounced GAG depletion and cytotoxic effects [74]. Such outcomes may arise from residual SDS remaining bound to ECM proteins [73, 74] or SDS-induced alterations to matrix biochemistry and structure [104]. Nevertheless, the cytotoxicity associated with SDS appears to be tissue- and protocol-dependent [23]. Together, these findings suggest that the use of SDS requires careful control of residual detergent and may be less suitable when matrix preservation and cytocompatibility are priorities. In contrast, a 2 d treatment with 1% Triton X-100 and 0.1% NH_4OH achieved thorough removal of cellular material while preserving key structural and biochemical features of the ECM, particularly collagen and GAG, in agreement with previous reports [5, 24]. Here, detergent-based protocols were investigated as practical methods for preparing cartilage dECM for downstream hydrogel fabrication. Enzymatic methods may assist cellular removal, but they are often used in combination with other treatments because proteolytic enzymes can also damage structural and bioactive ECM components [105]. Physical approaches, such as freeze–thaw, avoid chemical residues and may preserve some matrix features, but their effectiveness in dense tissues such as cartilage is often limited when used alone, while methods such as ultrasound may disrupt major structural fibres [2]. Overall, these findings identify 1% Triton–0.1% NH_4OH as the most suitable protocol among those tested here. Future studies may further explore enzymatic and physical approaches to determine whether additional improvements in decellularisation efficiency and matrix preservation can be achieved.

Comparative proteomic profiling further supported the selection of the 1% Triton–0.1% NH_4OH condition, showing reduced non-matrisome proteins together with better preservation of ECM-related proteins. Specifically, this condition was associated with increased abundance of proteins associated with cell proliferation (e.g. TGF-β1, COMP, FN, DCN, and PRG4) and chondrogenic differentiation (e.g. ACAN, COL2A1, FGF2, PRG4, and MATN3). These findings are consistent with previous studies suggesting that key matrisome biomolecules play important roles in maintaining chondrocyte phenotype and cartilage mechanical properties [69, 103, 106, 107]. Biomolecules such as COL2A1, FGF2 and ACAN are recognised as important regulators of chondrogenesis [108, 109]. Together, these findings suggest that improved preservation of cartilage-associated ECM cues may help explain the enhanced proliferation and chondrogenic responses of encapsulated hBMSCs observed in the absence of exogenous growth factors [103, 106]. Therefore, 1% Triton–0.1% NH_4OH was selected as the optimised decellularisation protocol for subsequent cellular studies.

All cell-laden hydrogels share a common fabrication dilemma of needing to be gently printable yet rapidly self-supporting, and self-crosslinking dECM is no exception [20]. Its slow gelation and limited stiffness often necessitate additional functionalisation or secondary crosslinking, introducing extra processing steps. A Ru/SPS photoinitiator system was applied to a biocompatible and consistently prepared dECM that maintained key matrix components, thereby improving its handling characteristics [6]. This chemistry enables rapid hydrogel formation within minutes without relying on collagen fibrillogenesis. Maintaining relatively low concentrations to reduce premature fibrillogenesis enables gelation to occur with reduced dependence on variables such as temperature, pH, ionic strength, and dECM concentration, which are often difficult to tightly control. Mechanical stiffness, in contrast, can be tuned

by adjusting the photoinitiator concentration. In this process, dECM proteins are co-crosslinked via existing tyrosine sites but are not chemically modified by new functional groups or highly reactive radicals [6], so the post-gelation protein composition still reflects the native dECM. In contrast, methacrylate functionalisation of pepsin-solubilised dECM hydrogels has been reported to impair their chondro-inductive capacity and fail to enhance hBMSC chondrogenesis [110]. Thus, the photo-crosslinked cartilage dECM hydrogel functions as a physiological depot, combining stable gradients of endogenous growth factors and tunable mechanical stiffness to regulate hBMSCs proliferation and differentiation towards the chondrocyte lineage [111].

We further demonstrated that the photo-crosslinked cartilage dECM hydrogels better preserve the articular chondrocyte phenotype of hBMSC-derived chondrocytes compared with GelMA. The expression of key chondrogenic marker genes, including *SOX9*, *ACAN*, and *COL2A1*, was significantly higher in the photo-crosslinked cartilage dECM hydrogels than in the GelMA, consistent with previous reports [3]. Notably, the *COL2*/*COL1* ratio, which is an established indicator of differentiated, hyaline-like articular cartilage phenotype [112], was also elevated in the dECM hydrogel.

A hypoxic microenvironment is essential for preserving the chondrogenic potential of hBMSCs and recapitulating the native cartilage niche, in which low oxygen tension promotes matrix synthesis and supports a non-hypertrophic phenotype [113]. In our system, we aimed to engineer hydrogels that can establish and maintain localised hypoxia by incorporating an oxygen scavenger while still supporting efficient oxygen-dependent photo-crosslinking during gel formation. However, achieving reliable hydrogel formation with localised oxygen control can be challenging, as efficient photo-crosslinking does not occur under anaerobic conditions [18]. While singlet oxygen may not directly interact with functional groups, oxygen nevertheless plays an essential role in driving the photo-oxidation and crosslinking of hydroxyphenyl, sulphide, and amine groups in the Ru/SPS-photo-mediated redox system [17]. This intrinsic dependence on oxygen complicates the development of a unified, hypoxia-compatible biofabrication strategy. To maintain shape fidelity for 3D culture while enabling localised oxygen control in conventional CO_2 incubators, the choice of oxygen scavenger is therefore critical. The oxygen scavenger, Oxyrase, previously used to generate localised hypoxia in a microgel system [16], interfered with the Ru/SPS-mediated photo-crosslinking in our photo-crosslinked cartilage dECM hydrogels and did not support the formation of robust cell-laden hydrogels (data not shown), which may be related to its instantaneous reaction kinetics. In contrast, oxygen-scavenging microcapsules containing glucose oxidase and catalase were compatible with our photo-crosslinking system, as their activity is glucose-dependent. In this case, the oxygen-consuming reaction is not initiated until the hydrogels are immersed in glucose-containing culture medium, which occurs after the rapid visible light-induced crosslinking. This strategy permits the preparation of cell-laden hydrogels with controllable biophysical and biochemical features by varying the concentrations of dECM and photoinitiator, and, importantly, allows modulation of the local oxygen tension by incorporating oxygen-scavenging microcapsules at different concentrations. The oxygen-scavenging effect is mediated by a glucose oxidase/catalase cascade, but the system also has several inherent limitations. Its activity depends on glucose availability and may therefore be influenced by media formulation and replenishment timing. In addition, because gluconic acid is generated during the reaction, potential pH changes should be considered during extended culture. Although no obvious macroscopic change in the culture medium was observed, pH was not directly monitored in the present study, and subtle or local microenvironmental changes cannot be excluded. The performance of the system may also be affected by transport-related factors, including diffusion across the capsule shell, oxygen resupply from the surrounding environment, and capsule concentration or spatial distribution. Accordingly, while functional oxygen regulation was confirmed within the biologically relevant culture window of this study, the longer-term behaviour of the system under the present construct and culture conditions requires further investigation.

In this study, our findings demonstrate that hypoxic dECM hydrogels integrated with oxygen-scavenging microcapsules can establish a hypoxia-mimetic microenvironment, thereby eliciting hypoxia responses in hBMSC-derived chondrocytes cultured in a conventional incubator. This was evidenced by increased expression and nuclear translocation of HIF-1α, a key regulator of hypoxia response. The enhanced nuclear activity of HIF-1α was associated with an articular phenotype in hBMSC-derived chondrocytes. Mechanistically, activation of SOX9 by HIF-1α promotes chondrogenic differentiation and stimulates the synthesis of major cartilage matrix proteins, including type II collagen and aggrecan [114]. In addition, TGF-β/SMAD2/3-related signalling under hypoxic conditions has been associated with increased anabolic activity of SOX5/6/9 and reduced hypertrophic differentiation, as reflected by RUNX2/COL10A1 expression [89]. By contrast, hBMSC-derived chondrocytes encapsulated within normoxic hydrogels displayed a hypertrophic phenotype, likely linked to elevated TNF-α/NF-κB signalling and Hedgehog pathway activation, which together facilitate the expression of matrix-degrading

enzymes such as MMPs and ADAMTS, leading to an inflammatory, catabolic state and favouring hypertrophy and endochondral ossification [91, 92]. The effects of hypoxia on Hedgehog and TNF/NF-κB signalling are highly tissue- and context-dependent. In articular cartilage, HIF-1α has been reported to preserve cartilage homeostasis through suppression of NF-κB signalling [115]. In broader inflammatory settings, HIF-1α has also been shown to restrict NF-κB transcriptional activity [116]. However, distinct responses have been described in other cell types. Hypoxia-associated HIF-1α signalling has been linked to enhanced neutrophil survival together with NF-κB-related activity [117], while HIF-1α accumulation is required for induction of the Hedgehog response in cardiomyoblasts and fibroblasts [118]. In addition, hypoxia can promote TNF-α/NF-κB signalling in cancer [119, 120]. Taken together, these findings indicate that hypoxic regulation of Hedgehog and TNF-α/NF-κB pathways is not uniform across tissues. Therefore, the changes observed in our study are more appropriately interpreted as a cartilage-specific response under our experimental conditions, rather than as a universal consequence of hypoxia. A limitation of the present study is that only hBMSCs were evaluated in the system, without the inclusion of primary chondrocytes. In future work, primary chondrocytes and other relevant stem cell sources will be included for direct comparison to better define cell source-dependent responses in this system.

In the current study, the photo-crosslinked 1% cartilage dECM hydrogel exhibited a stiffness range of 12.9–33.3 kPa, which is substantially lower than that of patient-derived cartilage, typically in the range of MPa [121]. Nevertheless, the relevance of this stiffness range to early cartilage regeneration should be interpreted in a context-dependent manner, as previous studies have shown that the relationship between matrix stiffness and chondrogenesis depends on hydrogel composition, crosslinking chemistry, cell source, matrix ligands, and culture conditions. For example, it has been suggested that the stiffness of developing cartilage may initially remain relatively low, with subsequent matrix deposition contributing to progressive maturation toward a more cartilage-like phenotype [122]. Consistent with this, hydrogels with stiffnesses in the range of 7–33 kPa have been reported to support a comparable degree of neocartilage formation, provided that a minimum initial stiffness is maintained to preserve structural integrity over time [123]. In addition, soft matrices of approximately 1 kPa have been shown to promote MSC chondrogenic differentiation [122], whereas other studies have suggested that higher stiffness values, such as ∼80 kPa, may also support hBMSC chondrogenic differentiation [124]. Together, these findings indicate that a clearly defined stiffness range for guiding chondrogenic differentiation remains under debate, and further studies are needed to determine the most appropriate stiffness range for MSCs or chondrocytes. In terms of mechanical enhancement, simply increasing the concentration of photoinitiator (Ru/SPS) may generate cytotoxic radicals and compromise cell viability, while different cell types may also display distinct tolerance to photoinitiator exposure and the resulting changes in stiffness [125]. Alternative approaches, including increasing dECM concentration, optimising crosslinking duration or network structure, and incorporating dual-network or composite reinforcement strategies, may therefore provide more effective routes to improve stiffness while preserving biological functionality in future studies [126, 127].

5. Conclusion

In this study, we developed a hypoxia-compatible photo-crosslinking strategy for dECM-based hydrogels, enabling robust hydrogel formation while preserving a low-oxygen microenvironment relevant to cartilage tissue. By integrating oxygen-scavenging microcapsules into the photo-crosslinking process, we successfully overcame the intrinsic incompatibility between radical-based photoinitiators and oxygen, achieving reliable gelation and spatiotemporal control of oxygen tension. Under hypoxic conditions, hBMSC-derived chondrocytes exhibited enhanced metabolic adaptation toward glycolysis, up-regulation of cartilage-anabolic and articular phenotype-associated genes, and attenuation of inflammatory, catabolic, and hypertrophy-related signalling. These molecular changes collectively support the acquisition of an articular-like, anabolic, and non-hypertrophic chondrocyte phenotype within the engineered microenvironment. Taken together, this work establishes a versatile biofabrication platform for constructing hypoxia-regulated, dECM-based cartilage models, providing a promising strategy for engineering physiologically relevant cartilage tissues for tissue engineering, disease modelling, and drug screening.

Acknowledgments

This work was supported by the NHMRC Investigator Grant Fellowship (APP1176298) awarded to I.P. L.L. is supported by an Australian Research Training Program (RTP) Scholarship. We acknowledge Queensland University of Technology (QUT) for providing subsidised access to specialised research infrastructure, including high-performance computing (HPC), and support from QUT's Digital Research Infrastructure team.

Data availability statement

All data that support the findings of this study are included within the article (and any supplementary files).

Author contributions

Lin Li 0009-0007-7945-4345
Conceptualization (equal), Data curation (equal), Formal analysis (lead), Investigation (lead), Methodology (lead), Validation (equal), Visualization (lead), Writing – original draft (lead), Writing – review & editing (equal)

Louis Jun Ye Ong 0000-0003-2398-7672
Conceptualization (supporting), Data curation (supporting), Investigation (supporting), Methodology (supporting), Project administration (supporting), Supervision (supporting), Visualization (supporting), Writing – review & editing (supporting)

Khoon S Lim 0000-0002-2486-196X
Conceptualization (supporting), Data curation (supporting), Methodology (equal)

Chamikara Liyanage 0000-0003-1542-5100
Data curation (supporting), Formal analysis (supporting), Methodology (supporting), Validation (supporting)

Yunkun Qu 0000-0002-8529-0478
Data curation (supporting), Formal analysis (supporting), Methodology (supporting)

Jingyi Wen 0000-0003-0926-0645
Data curation (supporting), Formal analysis (supporting), Investigation (supporting), Methodology (supporting)

Caitlin Williams 0000-0003-2681-2085
Methodology (supporting)

Thomas G Molley 0000-0001-8583-5397
Data curation (supporting), Methodology (supporting), Writing – review & editing (supporting)

Roberto A Barrero 0000-0002-7735-665X
Data curation (supporting), Formal analysis (supporting), Methodology (supporting), Writing – review & editing (supporting)

Shital Wakale 0009-0001-3667-3317
Formal analysis (supporting), Methodology (supporting)

Ross Crawford 0000-0001-6079-1316
Data curation (supporting)

Kristopher A Kilian 0000-0002-8963-9796
Data curation (supporting)

Yi-Chin Toh 0000-0002-4105-4852
Conceptualization (supporting), Project administration (supporting), Supervision (supporting), Visualization (supporting), Writing – review & editing (equal)

Indira Prasadam 0000-0001-5057-2427
Conceptualization (lead), Funding acquisition (lead), Project administration (lead), Supervision (lead), Writing – review & editing (equal)

References

[1] Golebiowska A A, Intravaia J T, Sathe V M, Kumbar S G and Nukavarapu S P 2024 Decellularized extracellular matrix biomaterials for regenerative therapies: advances, challenges and clinical prospects *Bioact. Mater.* **32** 98–123
[2] Xu J, Jiang N, Zhu S, Alini M, Grad S, Geurts J and Li Z 2025 Decellularized extracellular matrix-based hydrogels for cartilage repair and regeneration *Adv. Orthop.* **1** 83–97
[3] Chen Y-W, Lin Y-H, Lin T-L, Lee K-X A, Yu M-H and Shie M-Y 2023 3D-biofabricated chondrocyte-laden decellularized extracellular matrix-contained gelatin methacrylate auxetic scaffolds under cyclic tensile stimulation for cartilage regeneration *Biofabrication* **15** 045007
[4] Almalla A *et al* 2023 Papain-based solubilization of decellularized extracellular matrix for the preparation of bioactive, thermosensitive pregels *Biomacromolecules* **24** 5620–37
[5] Milton L A, Davern J W, Hipwood L, Chaves J C, McGovern J, Broszczak D, Hutmacher D W, Meinert C and Toh Y-C 2024 Liver click dECM hydrogels for engineering hepatic microenvironments *Acta Biomater.* **185** 144–60
[6] Kim H, Kang B, Cui X, Lee S-H, Lee K, Cho D-W, Hwang W, Woodfield T B F, Lim K S and Jang J 2021 Light-activated decellularized extracellular matrix-based bioinks for volumetric tissue analogs at the centimeter scale *Adv. Funct. Mater.* **31** 2011252
[7] Yu T-H, Yeh T-T, Su C-Y, Yu N-Y, Chen I-C and Fang H-W 2022 Preparation and characterization of extracellular matrix hydrogels derived from acellular cartilage tissue *J. Funct. Biomater.* **13** 279
[8] Lee A, Hudson A, Shiwarski D, Tashman J, Hinton T, Yerneni S, Bliley J, Campbell P and Feinberg A 2019 3D bioprinting of collagen to rebuild components of the human heart *Science* **365** 482–7
[9] Sharma N S, Karan A, Tran H Q, John J V, Andrabi S M, Shahriar S S and Xie J 2024 Decellularized extracellular matrix-decorated 3D nanofiber scaffolds enhance cellular responses and tissue regeneration *Acta Biomater.* **184** 81–97
[10] Ravichandran A, Murekatete B, Moedder D, Meinert C and Bray L J 2021 Photocrosslinkable liver extracellular matrix hydrogels for the generation of 3D liver microenvironment models *Sci. Rep.* **11** 15566
[11] Gonen-Wadmany M, Goldshmid R and Seliktar D 2011 Biological and mechanical implications of PEGylating proteins into hydrogel biomaterials *Biomaterials* **32** 6025–33
[12] Lim K S, Klotz B J, Lindberg G C J, Melchels F P W, Hooper G J, Malda J, Gawlitta D and Woodfield T B F 2019 Visible light cross-linking of gelatin hydrogels offers an enhanced cell microenvironment with improved light penetration depth *Macromol. Biosci.* **19** e1900098

[13] Sharifi S, Sharifi H, Akbari A and Chodosh J 2021 Systematic optimization of visible light-induced cross-linking conditions of gelatin methacryloyl (GelMA) *Sci. Rep.* **11** 23276

[14] Paul S, Schrobback K, Tran P A, Meinert C, Davern J W, Weekes A and Klein T J 2023 Photo-cross-linkable, injectable, and highly adhesive gelma-glycol chitosan hydrogels for cartilage repair *Adv. Healthcare Mater.* **12** 2302078

[15] Pattappa G, Markway B D, Docheva D and Johnstone B 2023 Physioxic culture of chondrogenic cells *Cartilage Tissue Engineering* (Springer) pp 45–63

[16] Ong L J Y, Sun A R, Wang Z, Lee J, Prasadam I and Toh Y C 2024 Localized oxygen control in a microfluidic osteochondral interface model recapitulates bone–cartilage crosstalk during osteoarthritis *Adv. Funct. Mater.* **34** 2315608

[17] Lim K S, Galarraga J H, Cui X, Lindberg G C J, Burdick J A and Woodfield T B F 2020 Fundamentals and applications of photo-cross-linking in bioprinting *Chem. Rev.* **120** 10662–94

[18] Spikes J D, Shen H R, Kopečková P and Kopeček J 1999 Photodynamic crosslinking of proteins. III. Kinetics of the FMN-and rose bengal-sensitized photooxidation and intermolecular crosslinking of model tyrosine-containing N-(2-hydroxypropyl) methacrylamide copolymers *Photochem. Photobiol.* **70** 130–7

[19] Bagheri A and Jin J 2019 Photopolymerization in 3D printing *ACS Appl. Polym. Mater.* **1** 593–611

[20] Kang B, Park Y, Hwang D G, Kim D, Yong U, Lim K S and Jang J 2022 Facile bioprinting process for fabricating size-controllable functional microtissues using light-activated decellularized extracellular matrix-based bioinks *Adv. Mater. Technol.* **7** 2100947

[21] Molley T G, Jiang S, Ong L, Kopecky C, Ranaweera C D, Jalandhra G K, Milton L, Kardia E, Zhou Z and Rnjak-Kovacina J 2023 Gas-modulating microcapsules for spatiotemporal control of hypoxia *Proc. Natl Acad. Sci. USA* **120** e2217557120

[22] Zeng J, Huang L, Xiong H, Li Q, Wu C, Huang Y, Xie H and Shen B 2022 Injectable decellularized cartilage matrix hydrogel encapsulating urine-derived stem cells for immunomodulatory and cartilage defect regeneration *npj Regen. Med.* **7** 75

[23] Jin Y, Kim H, Min S, Choi Y S, Seo S J, Jeong E, Kim S K, Lee H-A, Jo S-H and Park J-H 2022 Three-dimensional heart extracellular matrix enhances chemically induced direct cardiac reprogramming *Sci. Adv.* **8** eabn5768

[24] Jeong W, Kim M K and Kang H-W 2021 Effect of detergent type on the performance of liver decellularized extracellular matrix-based bio-inks *J. Tissue Eng.* **12** 2041731421997091

[25] Moffat D, Ye K and Jin S 2022 Decellularization for the retention of tissue niches *J. Tissue Eng.* **13** 20417314221101151

[26] Lu Y, Wang Y, Zhang H, Tang Z, Cui X, Li X, Liang J, Wang Q, Fan Y and Zhang X 2021 Solubilized cartilage ECM facilitates the recruitment and chondrogenesis of endogenous BMSCs in collagen scaffolds for enhancing microfracture treatment *ACS Appl. Mater. Interfaces* **13** 24553–64

[27] Fan X *et al* 2022 The deterioration of calcified cartilage integrity reflects the severity of osteoarthritis—a structural, molecular, and biochemical analysis *FASEB J.* **36** e22142

[28] Oliver W C and Pharr G M 1992 An improved technique for determining hardness and elastic modulus using load and displacement sensing indentation experiments *J. Mater. Res.* **7** 1564–83

[29] Daphalapurkar N, Wang F, Fu B, Lu H and Komanduri R 2011 Determination of mechanical properties of sand grains by nanoindentation *Exp. Mech.* **51** 719–28

[30] Zougman A, Selby P J and Banks R E 2014 Suspension trapping (STrap) sample preparation method for bottom-up proteomics analysis *Proteomics* **14** 1006–10

[31] Wu X, Fan X, Crawford R, Xiao Y and Prasadam I 2022 The metabolic landscape in osteoarthritis *Aging Dis.* **13** 1166–82

[32] Wakale S, Chen Y, Sun A R, Liyanage C, Gunter J, Batra J, Crawford R, Sang H and Prasadam I 2025 Comparative analysis of the therapeutic potential of extracellular vesicles secreted by aged and young bone marrow-derived mesenchymal stem cells in osteoarthritis pathogenesis *Cell Prolif.* **58** e13776

[33] Liyanage C, Malik A, Abeysinghe P, Clements J and Batra J 2021 SWATH-MS based proteomic profiling of prostate cancer cells reveals adaptive molecular mechanisms in response to anti-androgen therapy *Cancers* **13** 715

[34] Yang Y, Bagnaninchi P O, Ahearne M, Wang R K and Liu K-K 2007 A novel optical coherence tomography-based micro-indentation technique for mechanical characterization of hydrogels *J. R. Soc. Interface* **4** 1169–73

[35] Hertz H 1882 On the contact of rigid elastic solids and on hardness *Assorted Papers by H. Hertz* (MacMillan) pp 156–71

[36] Monteiro N, Thrivikraman G, Athirasala A, Tahayeri A, França C M, Ferracane J L and Bertassoni L E 2018 Photopolymerization of cell-laden gelatin methacryloyl hydrogels using a dental curing light for regenerative dentistry *Dent. Mater.* **34** 389–99

[37] Cui X *et al* 2020 Rapid photocrosslinking of silk hydrogels with high cell density and enhanced shape fidelity *Adv. Healthcare Mater.* **9** 1901667

[38] Prasadam I, Akuien A, Friis T E, Fang W, Mao X, Crawford R W and Xiao Y 2018 Mixed cell therapy of bone marrow-derived mesenchymal stem cells and articular cartilage chondrocytes ameliorates osteoarthritis development *Lab. Invest.* **98** 106–16

[39] Farnaghi S, Crawford R, Xiao Y and Prasadam I 2017 Cholesterol metabolism in pathogenesis of osteoarthritis disease *Int. J. Rheum. Dis.* **20** 131–40

[40] Schutze N, Noth U, Schneidereit J, Hendrich C and Jakob F 2005 Differential expression of CCN-family members in primary human bone marrow-derived mesenchymal stem cells during osteogenic, chondrogenic and adipogenic differentiation *Cell Commun. Signal.* **3** 5

[41] Loessner D, Meinert C, Kaemmerer E, Martine L C, Yue K, Levett P A, Klein T J, Melchels F P W, Khademhosseini A and Hutmacher D W 2016 Functionalization, preparation and use of cell-laden gelatin methacryloyl–based hydrogels as modular tissue culture platforms *Nat. Protocols* **11** 727–46

[42] Milton L A *et al* 2025 Building multiple microenvironmental niches using a customizable 3D printed well insert *Lab Chip* **25** 5875–93

[43] Ewels P A, Peltzer A, Fillinger S, Patel H, Alneberg J, Wilm A, Garcia M U, Di Tommaso P and Nahnsen S 2020 The nf-core framework for community-curated bioinformatics pipelines *Nat. Biotechnol.* **38** 276–8

[44] Zhong X, Heinicke F and Rayner S 2019 miRBaseMiner, a tool for investigating miRBase content *RNA Biol.* **16** 1534–46

[45] Love M I, Huber W and Anders S 2014 Moderated estimation of fold change and dispersion for RNA-seq data with DESeq2 *Genome Biol.* **15** 550

[46] Sello C T *et al* 2019 De novo assembly and comparative transcriptome profiling of Anser anser and Anser cygnoides geese species' embryonic skin feather follicles *Genes* **10** 351

[47] Wu T *et al* 2021 clusterProfiler 4.0: a universal enrichment tool for interpreting omics data *Innovation* **2** 100141

[48] Subramanian A *et al* 2005 Gene set enrichment analysis: a knowledge-based approach for interpreting genome-wide expression profiles *Proc. Natl Acad. Sci. USA* **102** 15545–50

[49] Higuita M L and Griffiths L G 2020 Antigen removal process preserves function of small diameter venous valved conduits, whereas SDS-decellularization results in significant valvular insufficiency *Acta Biomater.* **107** 115–28

[50] Kang D, Lee J, Yook G, Jeong S, Shin J, Kim M-S, Kim Y-J, Jung H, Ahn J and Kim T W 2025 Regulation of senescence-associated secretory phenotypes in osteoarthritis by cytosolic UDP-GlcNAc retention and O-GlcNAcylation *Nat. Commun.* **16** 1094
[51] Yang B *et al* 2025 Recapitulating hypoxic metabolism in cartilaginous organoids via adaptive cell-matrix interactions enhances histone lactylation and cartilage regeneration *Nat. Commun.* **16** 2711
[52] Lin W and Klein J 2021 Recent progress in cartilage lubrication *Adv. Mater.* **33** 2005513
[53] Luo Y, Sinkeviciute D, He Y, Karsdal M, Henrotin Y, Mobasheri A, Önnerfjord P and Bay-Jensen A 2017 The minor collagens in articular cartilage *Protein Cell* **8** 560–72
[54] Junqueira L C U, Bignolas G and Brentani R R 1979 Picrosirius staining plus polarization microscopy, a specific method for collagen detection in tissue sections *Histochem. J.* **11** 447–55
[55] Hwang J, San B H, Turner N J, White L J, Faulk D M, Badylak S F, Li Y and Yu S M 2017 Molecular assessment of collagen denaturation in decellularized tissues using a collagen hybridizing peptide *Acta Biomater.* **53** 268–78
[56] Khanarian N T, Boushell M K, Spalazzi J P, Pleshko N, Boskey A L and Lu H H 2014 FTIR-I compositional mapping of the cartilage-to-bone interface as a function of tissue region and age *J. Bone Miner. Res.* **29** 2643–52
[57] Listrat A, Boby C, Tournayre J and Jousse C 2023 Bovine extracellular matrix proteins and potential role in meat quality: first in silico Bos taurus compendium *J. Proteomics* **279** 104891
[58] Naba A 2024 Mechanisms of assembly and remodelling of the extracellular matrix *Nat. Rev. Mol. Cell Biol.* **25** 865–85
[59] Naba A, Clauser K R, Hoersch S, Liu H, Carr S A and Hynes R O 2012 The matrisome: in silico definition and *in vivo* characterization by proteomics of normal and tumor extracellular matrices *Mol. Cell. Proteomics* **11** M111.014647
[60] Bertels J C, He G and Long F 2024 Metabolic reprogramming in skeletal cell differentiation *Bone Res.* **12** 57
[61] Linkova N, Khavinson V, Diatlova A, Myakisheva S and Ryzhak G 2023 Peptide regulation of chondrogenic stem cell differentiation *Int. J. Mol. Sci.* **24** 8415
[62] Iaquinta M R *et al* 2021 The role of microRNAs in the osteogenic and chondrogenic differentiation of mesenchymal stem cells and bone pathologies *Theranostics* **11** 6573–91
[63] Sulcanese L, Prencipe G, Canciello A, Cerveró-Varona A, Perugini M, Mauro A, Russo V and Barboni B 2024 Stem-cell-driven chondrogenesis: perspectives on amnion-derived cells *Cells* **13** 744
[64] Yang X, Tian S, Fan L, Niu R, Yan M, Chen S, Zheng M and Zhang S 2022 Integrated regulation of chondrogenic differentiation in mesenchymal stem cells and differentiation of cancer cells *Cancer Cell Int.* **22** 169
[65] Green J D, Tollemar V, Dougherty M, Yan Z, Yin L, Ye J, Collier Z, Mohammed M K, Haydon R C and Luu H H 2015 Multifaceted signaling regulators of chondrogenesis: implications in cartilage regeneration and tissue engineering *Genes Dis.* **2** 307–27
[66] Kozhemyakina E, Lassar A B and Zelzer E 2015 A pathway to bone: signaling molecules and transcription factors involved in chondrocyte development and maturation *Development* **142** 817–31
[67] Li J and Dong S 2016 The signaling pathways involved in chondrocyte differentiation and hypertrophic differentiation *Stem Cells Int.* **2016** 2470351
[68] Wuelling M and Vortkamp A 2010 Transcriptional networks controlling chondrocyte proliferation and differentiation during endochondral ossification *Pediatr. Nephrol.* **25** 625–31
[69] Chen H, Tan X-N, Hu S, Liu R-Q, Peng L-H, Li Y-M and Wu P 2021 Molecular mechanisms of chondrocyte proliferation and differentiation *Front. Cell Dev. Biol.* **9** 664168
[70] Wuelling M and Vortkamp A 2011 Chondrocyte proliferation and differentiation *Endocr. Dev.* **21** 1–11
[71] Meek K M 2009 Corneal collagen—its role in maintaining corneal shape and transparency *Biophys. Rev.* **1** 83–93
[72] Roshanbinfar K, Evans A D, Samanta S, Kolesnik-Gray M, Fiedler M, Krstic V, Engel F B and Oommen O P 2025 Enhancing biofabrication: shrink-resistant collagen-hyaluronan composite hydrogel for tissue engineering and 3D bioprinting applications *Biomaterials* **318** 123174
[73] Bongolan T, Whiteley J, Castillo-Prado J, Fantin A, Larsen B, Wong C J, Mazilescu L, Kawamura M, Urbanellis P and Jonebring A 2022 Decellularization of porcine kidney with submicellar concentrations of SDS results in the retention of ECM proteins required for the adhesion and maintenance of human adult renal epithelial cells *Biomater. Sci.* **10** 2972–90
[74] Fernández-Pérez J and Ahearne M 2019 The impact of decellularization methods on extracellular matrix derived hydrogels *Sci. Rep.* **9** 14933
[75] Castilho M, Levato R, Bernal P N, de Ruijter M, Sheng C Y, van Duijn J, Piluso S, Ito K and Malda J 2021 Hydrogel-based bioinks for cell electrowriting of well-organized living structures with micrometer-scale resolution *Biomacromolecules* **22** 855–66
[76] Zhou C, Wang C, Xu K, Niu Z, Zou S, Zhang D, Qian Z, Liao J and Xie J 2023 Hydrogel platform with tunable stiffness based on magnetic nanoparticles cross-linked GelMA for cartilage regeneration and its intrinsic biomechanism *Bioact. Mater.* **25** 615–28
[77] Pitsillides A A and Beier F 2021 Keep your Sox on, chondrocytes! *Nat. Rev. Rheumatol.* **17** 383–4
[78] Yang P *et al* 2024 Targeting Fascin1 maintains chondrocytes phenotype and attenuates osteoarthritis development *Bone Res.* **12** 50
[79] Yang Y, Wu Y, Yang D, Neo S H, Kadir N D, Goh D, Tan J X, Denslin V, Lee E H and Yang Z 2023 Secretive derived from hypoxia preconditioned mesenchymal stem cells promote cartilage regeneration and mitigate joint inflammation via extracellular vesicles *Bioact. Mater.* **27** 98–112
[80] Markway B D, Cho H and Johnstone B 2013 Hypoxia promotes redifferentiation and suppresses markers of hypertrophy and degeneration in both healthy and osteoarthritic chondrocytes *Arthritis Res. Ther.* **15** R92
[81] Grimmer C, Balbus N, Lang U, Aigner T, Cramer T, Müller L, Swoboda B and Pfander D 2006 Regulation of type II collagen synthesis during osteoarthritis by prolyl-4-hydroxylases: possible influence of low oxygen levels *Am. J. Pathol.* **169** 491–502
[82] Pap T and Korb-Pap A 2015 Cartilage damage in osteoarthritis and rheumatoid arthritis—two unequal siblings *Nat. Rev. Rheumatol.* **11** 606–15
[83] Lian C *et al* 2019 Collagen type II suppresses articular chondrocyte hypertrophy and osteoarthritis progression by promoting integrin β1− SMAD1 interaction *Bone Res.* **7** 8
[84] Aigner T, Söder S, Gebhard P M, McAlinden A and Haag J 2007 Mechanisms of disease: role of chondrocytes in the pathogenesis of osteoarthritis—structure, chaos and senescence *Nat. Clin. Pract. Rheumatol.* **3** 391–9
[85] van der Kraan P M and van den Berg W B 2012 Chondrocyte hypertrophy and osteoarthritis: role in initiation and progression of cartilage degeneration? *Osteoarthritis Cartilage* **20** 223–32
[86] Browe D C, Coleman C M, Barry F P and Elliman S J 2019 Hypoxia activates the PTHrP-MEF2C pathway to attenuate hypertrophy in mesenchymal stem cell derived cartilage *Sci. Rep.* **9** 13274
[87] Phillips R 2022 Articular cartilage hypoxia is a potential target for OA therapy *Nat. Rev. Rheumatol.* **18** 3
[88] Studer D, Millan C, Ozturk E, Maniura-Weber K and Zenobi-Wong M 2012 Molecular and biophysical mechanisms regulating hypertrophic differentiation in

chondrocytes and mesenchymal stem cells *Eur. Cell. Mater.* **24** 118–35
[89] Zhang T, Wen F, Wu Y, Goh G S H, Ge Z, Tan L P, Hui J H P and Yang Z 2015 Cross-talk between TGF-beta/SMAD and integrin signaling pathways in regulating hypertrophy of mesenchymal stem cell chondrogenesis under deferral dynamic compression *Biomaterials* **38** 72–85
[90] Xie M, Zhang Y, Xiong Z, Hines S, Shang J, Clark K L, Tan S, Alexander P G and Lin H 2022 Generation of hyaline-like cartilage tissue from human mesenchymal stromal cells within the self-generated extracellular matrix *Acta Biomater.* **149** 150–66
[91] Liao C-R, Wang S-N, Zhu S-Y, Wang Y-Q, Li Z-Z, Liu Z-Y, Jiang W-S, Chen J-T and Wu Q 2020 Advanced oxidation protein products increase TNF-α and IL-1β expression in chondrocytes via NADPH oxidase 4 and accelerate cartilage degeneration in osteoarthritis progression *Redox Biol.* **28** 101306
[92] Alman B A 2015 The role of hedgehog signalling in skeletal health and disease *Nat. Rev. Rheumatol.* **11** 552–60
[93] Chen Y *et al* 2022 Hnrnpk maintains chondrocytes survival and function during growth plate development via regulating Hif1α-glycolysis axis *Cell Death Dis.* **13** 803
[94] Guan P P, Ding W Y and Wang P 2018 The roles of prostaglandin F_2 in regulating the expression of matrix metalloproteinase-12 via an insulin growth factor-2-dependent mechanism in sheared chondrocytes *Signal Transduct. Target. Ther.* **3** 27
[95] Ji S and Guvendiren M 2017 Recent advances in bioink design for 3D bioprinting of tissues and organs *Front. Bioeng. Biotechnol.* **5** 23
[96] DeForest C A and Anseth K S 2012 Advances in bioactive hydrogels to probe and direct cell fate *Annu. Rev. Chem. Biomol.* **3** 421–44
[97] Kim B S, Das S, Jang J and Cho D-W 2020 Decellularized extracellular matrix-based bioinks for engineering tissue- and organ-specific microenvironments *Chem. Rev.* **120** 10608–61
[98] Elder B D, Kim D H and Athanasiou K A 2010 Developing an articular cartilage decellularization process toward facet joint cartilage replacement *Neurosurgery* **66** 722–7
[99] Yang Z, Shi Y, Wei X, He J, Yang S, Dickson G, Tang J, Xiang J, Song C and Li G 2010 Fabrication and repair of cartilage defects with a novel acellular cartilage matrix scaffold *Tissue Eng. C* **16** 865–76
[100] Benders K E, Boot W, Cokelaere S M, Van Weeren P R, Gawlitta D, Bergman H J, Saris D B F, Dhert W J A and Malda J 2014 Multipotent stromal cells outperform chondrocytes on cartilage-derived matrix scaffolds *Cartilage* **5** 221–30
[101] Sutherland A J and Detamore M S 2015 Bioactive microsphere-based scaffolds containing decellularized cartilage *Macromol. Biosci.* **15** 979–89
[102] Choudhury D, Yee M, Sheng Z L J, Amirul A and Naing M W 2020 Decellularization systems and devices: state-of-the-art *Acta Biomater.* **115** 51–59
[103] Cheng N-C, Estes B T, Awad H A and Guilak F 2009 Chondrogenic differentiation of adipose-derived adult stem cells by a porous scaffold derived from native articular cartilage extracellular matrix *Tissue Eng. A* **15** 231–41
[104] Gratzer P F, Harrison R D and Woods T 2006 Matrix alteration and not residual sodium dodecyl sulfate cytotoxicity affects the cellular repopulation of a decellularized matrix *Tissue Eng.* **12** 2975–83
[105] Nouri Barkestani M, Naserian S, Uzan G and Shamdani S 2021 Post-decellularization techniques ameliorate cartilage decellularization process for tissue engineering applications *J. Tissue Eng.* **12** 2041731420983562
[106] Rothrauff B B, Yang G and Tuan R S 2017 Tissue-specific bioactivity of soluble tendon-derived and cartilage-derived extracellular matrices on adult mesenchymal stem cells *Stem Cell Res. Ther.* **8** 133
[107] Chen Y, Sun W, Wen Y, Wang X, Li J, Xie S, Li R, Ma Y, Wu H and Zhu Q 2025 A cationic polymer drives glycosaminoglycan assembly and secretion for preclinical osteoarthritis therapy *Sci. Transl. Med.* **17** eadl5623
[108] Chen S, Tao J, Bae Y, Jiang M M, Bertin T, Chen Y, Yang T and Lee B 2013 Notch gain of function inhibits chondrocyte differentiation via Rbpj-dependent suppression of Sox9 *J. Bone Miner. Res.* **28** 649–59
[109] Chiu L H, Chen S-C, Wu K-C, Yang C-B, Fang C-L, Lai W-F T and Tsai Y-H 2011 Differential effect of ECM molecules on re-expression of cartilaginous markers in near quiescent human chondrocytes *J. Cell Physiol.* **226** 1981–8
[110] Rothrauff B B, Coluccino L, Gottardi R, Ceseracciu L, Scaglione S, Goldoni L and Tuan R S 2018 Efficacy of thermoresponsive, photocrosslinkable hydrogels derived from decellularized tendon and cartilage extracellular matrix for cartilage tissue engineering *J. Tissue Eng. Regen. Med.* **12** e159–70
[111] Hynes R O 2009 The extracellular matrix: not just pretty fibrils *Science* **326** 1216–9
[112] Albrecht C, Tichy B, Nürnberger S, Hosiner S, Zak L, Aldrian S and Marlovits S 2011 Gene expression and cell differentiation in matrix-associated chondrocyte transplantation grafts: a comparative study *Osteoarthritis Cartilage* **19** 1219–27
[113] Jiang Z *et al* 2025 Hypoxia, cuproptosis, and osteoarthritis: unraveling the molecular crosstalk *Redox Biol.* **85** 103757
[114] Duval E, Baugé C, Andriamanalijaona R, Bénateau H, Leclercq S, Dutoit S, Poulain L, Galéra P and Boumédiene K 2012 Molecular mechanism of hypoxia-induced chondrogenesis and its application in *in vivo* cartilage tissue engineering *Biomaterials* **33** 6042–51
[115] Okada K *et al* 2020 Hypoxia-inducible factor-1 alpha maintains mouse articular cartilage through suppression of NF-κB signaling *Sci. Rep.* **10** 5425
[116] D'Ignazio L, Bandarra D and Rocha S 2016 NF-κB and HIF crosstalk in immune responses *FEBS J.* **283** 413–24
[117] Walmsley S R *et al* 2011 Prolyl hydroxylase 3 (PHD3) is essential for hypoxic regulation of neutrophilic inflammation in humans and mice *J. Clin. Invest.* **121** 1053–63
[118] Bijlsma M F 2008 Hypoxia induces a hedgehog response mediated by HIF-1alpha *J. Cell. Mol. Med.* **13** 2053–60
[119] D'Ignazio L, Batie M and Rocha S 2017 Hypoxia and inflammation in cancer, focus on HIF and NF-κB *Biomedicines* **5** 21
[120] Oliver K M, Garvey J F, Ng C T, Veale D J, Fearon U, Cummins E P and Taylor C T 2009 Hypoxia activates NF-kappaB–dependent gene expression through the canonical signaling pathway *Antioxid. Redox Signal.* **11** 2057–64
[121] Eschweiler J, Horn N, Rath B, Betsch M, Baroncini A, Tingart M and Migliorini F 2021 The biomechanics of cartilage-an overview *Life* **11** 302
[122] Park J S, Chu J S, Tsou A D, Diop R, Tang Z, Wang A and Li S 2011 The effect of matrix stiffness on the differentiation of mesenchymal stem cells in response to TGF-β *Biomaterials* **32** 3921–30
[123] Wang T, Lai J H and Yang F 2016 Effects of hydrogel stiffness and extracellular compositions on modulating cartilage regeneration by mixed populations of stem cells and chondrocytes in vivo *Tissue Eng. A* **22** 1348–56
[124] Oh S H, An D B, Kim T H and Lee J H 2016 Wide-range stiffness gradient PVA/HA hydrogel to investigate stem cell differentiation behavior *Acta Biomater.* **35** 23–31

[125] Williams C G, Malik A N, Kim T K, Manson P N and Elisseeff J H 2005 Variable cytocompatibility of six cell lines with photoinitiators used for polymerizing hydrogels and cell encapsulation *Biomaterials* **26** 1211–8
[126] Fairbanks B D, Schwartz M P, Bowman C N and Anseth K S 2009 Photoinitiated polymerization of PGE-diacrylate with lithium phenyl-2,4,6-trimethylbenzoylphosphinate: polymerization rate and cytocompatibility *Biomaterials* **30** 6702–7
[127] Zhou Z, Song P, Wu Y, Wang M, Shen C, Ma Z, Ren X, Wang X, Chen X and Hu Y 2024 Dual-network DNA–silk fibroin hydrogels with controllable surface rigidity for regulating chondrogenic differentiation *Mater. Horiz.* **11** 1465–83